

CHARACTERIZING THE VEGETATIVE PHENOTYPE OF *fzt* MAIZE MUTANT

by

Christine Elizabeth Todd Basham

June 1st, 2012

Director: Dr. Beth Thompson

Major Department: Biology

microRNAs are short, non-coding RNA strands that regulate gene expression post-transcriptionally in all multicellular organisms. miRNAs begin as a hairpin in the nucleus. The primary miRNA (pri-miRNA) and preliminary miRNA (pre-miRNA) are cleaved by DICER-LIKE1 to form the miRNA, demonstrating this protein is essential for the proper biogenesis of miRNAs. Once the miRNA is formed, it regulates gene expression by mRNA cleavage or translation repression. *fzt* is a maize mutant with a missense mutation in DICER-LIKE1. The *fzt* mutant has abnormal vegetative and reproductive tissue phenotypes. My research focuses on the vegetative development of the mutant. The mutant plants are shorter in stature with shorter and narrower leaves compared to their normal siblings. miRNAs have well established roles in plant development, including establishing leaf polarity and phase change. A complex mechanism involving specific miRNAs establishes proper adaxial and abaxial leaf polarity, including miR390, miR165, and miR166. A balance of two known miRNAs promotes juvenile and adult characteristics; miR156 and miR172. Both of these developmental functions were analyzed in this project. We also investigated the difference in leaf size between the normal sibling and mutant plants by looking at cell size, cell number, and cell proliferation.

We found a difference in both the leaf polarity and phase change between the normal sibling and *fzt* mutant. Epidermal cell types in maize are surface-specific. We found an

adaxialization of the abaxial surface, as well as an abaxialization of the adaxial surface by scanning electron microscopy. This polarity defect was more severe in the Mo17-background mutant plants. We also found a subtle polarity defect in the vasculature of adult leaves in the Mo17-background. Phase change was analyzed using epidermal peels and Toluidine Blue O staining. In both the A619- and Mo17-backgrounds, we found an adult transition one-leaf early. The size difference of the normal sibling and mutant plants was examined by cell size measurements and cell counts using epidermal peels. Cell proliferation was analyzed by examining tubulin dynamics in the pre- and post-differentiation zones of adult maize leaves. Maize is an essential crop plant, and has recently been used to explore alternate fuel alternatives. Further understanding maize development could lead to an increase in yield, both ear and leaf tissue.

CHARACTERIZING THE VEGETATIVE PHENOTYPE OF *fzt* MAIZE MUTANT

A Thesis

Presented to

The Faculty of the Department of Biology

East Carolina University

In Partial Fulfillment

Of the Requirements for the Degree

Master of Science in Molecular Biology

by

Christine Elizabeth Basham

June 1st, 2012

© Copyright 2012

Christine Elizabeth Basham

PHENOTYPIC CHARACTERIZATION OF *ftz* MAIZE MUTANT

By

Christine Elizabeth Todd Basham

APPROVED BY:

DIRECTOR OF THESIS: _____

Beth Thompson, Ph.D

COMMITTEE MEMBER: _____

Tim Christensen, Ph.D

COMMITTEE MEMBER: _____

Baohang Zhang, Ph.D

COMMITTEE MEMBER: _____

Amanda Wright, Ph.D

CHAIR OF THE DEPARTMENT OF BIOLOGY: _____

Jeff McKinnon, Ph.D

DEAN OF THE GRADUATION SCHOOL: _____

Paul Gemperline, Ph. D

DEDICATION

I would like to dedicate this thesis to my parents, Jim and Brenda Todd. Without their continued love and support through all of my endeavors, academic and otherwise, I would not be where I am today.

ACKNOWLEDGEMENTS

I am extremely thankful to my advisor, Dr. Beth Thompson, whose encouragement, guidance, and support from the initial enabled me to develop an understanding of my project and grow immeasurably as a scientist.

For this project, I would also like to thank the members of my committee: Tim Christensen, Amanda Wright, and Baohang Zhang. Your time and insightful questions were always appreciated and valued.

In my daily work, I have been surrounded by a group of fellow students willing to help whenever possible. Sarah Thalhamer for providing encouragement, smiles, and a good break whenever needed. Ryan Vick for the best tutoring in Microsoft Office programs, “loopage” conversations, and answering my countless questions.

Lastly, I would like to thank my family for all their love and encouragement. To my parents, who raised me with a love of education and supported me in all my pursuits, in and out of the classroom. My brother who has been inspirational in his own education endeavors. And to my loving, supportive and encouraging husband, Jordan, whose support has been a solid rock through this program. I love you.

TABLE OF CONTENTS

LIST OF FIGURES	i
LIST OF TABLES	iii
CHARACTERIZING THE VEGETATIVE PHENOTYPE OF <i>fzt</i> MAIZE MUTANT	
1. Introduction.....	1
2. Materials and Methods.....	15
Greenhouse Plant Preparation.....	15
Growth Chamber Plant Preparation	16
Scanning Electron Microscopy (SEM).....	16
Hand Sections	17
Primer Design	17
RNA Extraction	18
cDNA Synthesis.....	19
Real Time-PCR.....	20
Glue Impressions	21
Epidermal Peels	22
Cell Size Measurements.....	22
Cell Counts.....	23
Propidium Iodide Staining	23
Tubulin Immunofluorescence	23
3. Results.....	26
Characterize Overall Vegetative <i>fzt</i> Phenotype	26
Plant Height	26
Tassel Branch Number.....	28
Leaf Number	30
Internode Length.....	32
Stem Area.....	34
Root Mass	36
Characterize Adaxial/Abaxial Polarity	39
Epidermal Cell Types	42
Vasculature Orientation	50

mRNA Levels of HD-ZIPs	52
Characterize Juvenile to Adult Transition	56
Analyze Leaf Cell Size and Number	65
Overall Leaf Size	65
Juvenile Cell Size.....	67
Adult Cell Size.....	69
4. Discussion.....	73
REFERENCES	78

LIST OF FIGURES

CHARACTERIZING THE VEGETATIVE PHENOTYPE OF *fzt* MAIZE MUTANT

1.01 - Simplified miRNA biogenesis.....	2
1.02 - <i>fzt</i> encodes <i>dcl1</i>	4
1.03 - Normal and <i>fzt</i> mature maize plants	5
1.04 - <i>fzt</i> Inflorescence Phenotype	6
1.05 - Leaf Axes.....	8
1.06 - Proper leaf polarity is established through a network of miRNA regulation	10
2.01 - qPCR efficiencies for all four experiments used in analysis	21
3.01 - Plant Height	27
3.02 - Tassel Branch Number	29
3.03 - Leaf Number Average	31
3.04 - Internode Length.....	33
3.05 - Stem Area	35
3.06 - Root Mass	37
3.07 - miRNA regulation of adaxial/abaxial polarity	40
3.08 - Normal Ligule Tissue	41
3.09 - Leaf Sample Locations	45
3.10 - Epidermal cells of normal and <i>fzt</i> plants in A619 inbred background	47
3.11 - Epidermal cells of normal and <i>fzt</i> plants in Mo17 inbred background.....	48
3.12 - Vasculature orientation of normal and <i>fzt</i> plants in Mo17 inbred background	51
3.13 - Gene expression data for three biological replicates of 2-week old seedlings	53
3.14 - Gene expression data for one biological replicate of 5-week old plants	55

3.15 - A619 Epidermal Peels	59
3.16 - Mo17 Epidermal Peels.....	61
3.17 - A619 Bulliform Rows	63
3.18 - Mo17 Bulliform Rows.....	64
3.19 - Leaf Length & Width Differences.....	66
3.20 - A619 Juvenile Leaf Measurements	68
3.21 - A619 Adult Cell Size Measurements	70
3.22 - Mo17 Adult Cell Size Measurements.....	71

LIST OF TABLES

CHARACTERIZING THE VEGETATIVE PHENOTYPE OF *fzt* MAIZE MUTANT

1.01 - Blade Epidermal Cell Types.....	11
1.02 - Sheath Epidermal Cell Types.....	12
2.01 - qPCR Primer Sequences.....	18
3.01 - Blade Epidermal Cell Types.....	43
3.02 - Sheath Epidermal Cell Types.....	44
3.03 - Juvenile and Adult Leaf Cell Characteristics.....	57

1. INTRODUCTION

microRNAs

miRNAs are short, non-coding RNAs, about 21 nucleotides long. These non-coding RNA strands repress gene expression post-transcriptionally in all multicellular organisms. miRNAs regulate various processes in both plants and animals including normal development, carcinogenesis, and stress responses [30, 16, 4]. In general, miRNAs repress gene expression by directing target mRNA cleavage or translational repression.

miRNAs are generated through a two-step process (**FIGURE 1.01**). miRNAs are transcribed as a long, primary RNA (pri-miRNA), which includes a hairpin structure, DICER-LIKE1 cleaves at the base of the hairpin, releasing the precursor miRNA (pre-miRNA). In plants, DCL1 also cleaves the pre-miRNA to release the miRNA/miRNA* small RNA duplex. HEN1 methylates the 3' ends of the miRNA sequence to protect the RNA from degradation. Helicase unwinds the miRNA:miRNA* duplex. One of these strands, miRNA*, is thought to be degraded, while the other half of the duplex is the active miRNA that joins the RNA-induced silencing complex (RISC). The miRNA anneals to a complementary mRNA sequence and the endonuclease protein of RISC, ARGONAUTE1 (AGO1), cleaves the complementary mRNA or inhibits translation [30, 16, 4].

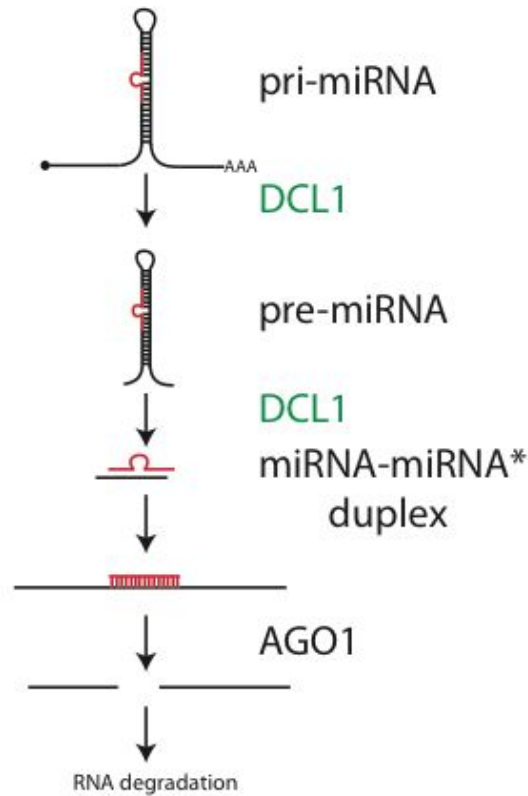


FIGURE 1.01.
Simplified miRNA
biogenesis
 Simplified miRNA
 biogenesis
 pathway,
 highlighting the
 two independent
 steps in which
 DICER-LIKE1
 (DCL1) functions.

This pathway differs from the miRNA biogenesis in animals in several respects. First, both cleavages in miRNA biogenesis in plants are performed in the nucleus. In animals, the first cleavage of the pri-miRNA is performed in the nucleus and the second cleavage of the pre-miRNA is performed in the cytoplasm [32, 30]. Another difference between plant and animal miRNA biogenesis is the protein involved in the cleavages. Both nuclear cleavages are processed by DICER-LIKE1 in plants, but in animals two different enzymes perform the nuclear and cytoplasmic cleavages [1]. Also in plants, HEN1 methylates the 3' ends of the miRNA sequences to protect the RNA from degradation [30].

miRNAs function to regulate multiple processes in development in both plants and animals. In both maize and Arabidopsis, miRNAs have well-established roles in regulating leaf polarity and phase change [5, 14, 15, 17, 6, 7]. Although little is known about the role miRNAs

play in cell proliferation in maize, in Arabidopsis, miR396 influences final organ size by repressing *GROWTH-REGULATING FACTORS (GRFS)* [27]. Overexpression of miR396 results in a reduced leaf size [27, 18].

fuzzy tassel

fuzzy tassel (fzt) is an EMS-induced mutant in maize with striking vegetative and reproductive tissue phenotypes (**FIGURE 1.03**); *fzt* is completely recessive and 100% penetrant. *fzt* was generated in the A619 inbred background, and has been backcrossed to both Mo17 and B73. The *fzt* phenotype is striking in all three backgrounds, although there are qualitative differences depending on the inbred background.

fzt was cloned using a map-based cloning approach. *fzt* maps to bin 1.01 on chromosome 1 to a region spanned by 3.2 cM (**FIGURE 1.02**) (B. Thompson, unpublished). Within this region, *dcl1* stood out as a particularly strong candidate due to the pleiotropic *fzt* phenotype and the well-known roles of miRNAs in many developmental processes. Indeed, *fzt* mutants harbors a G to A mutation in the *dcl1* cDNA, corresponding to exon 15. This mutation is predicted to cause S to N substitution in the first RNase III domain of DCL1 (B. Thompson, unpublished). *fzt* also fails to complement three putative null alleles of *fzt*, confirming that *fzt* is in fact an allele of *dcl1*.

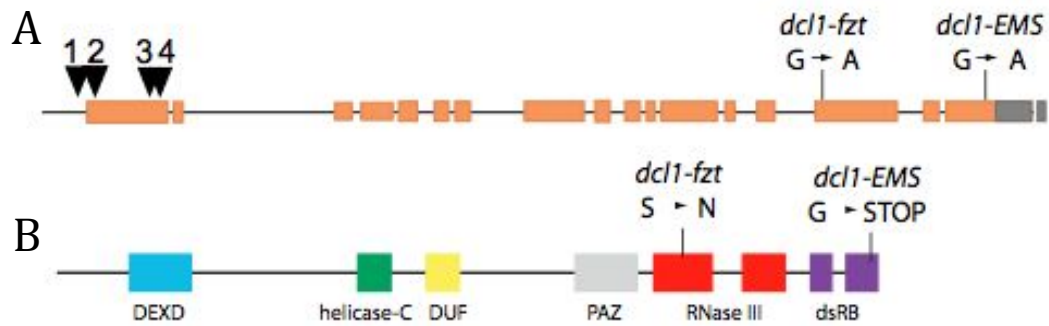


FIGURE 1.02. *fzt* encodes *dcl1*

A. genomic structure of *dcl1* locus. Orange boxes indicate coding regions and gray boxes indicate UTR. B. Structure of DCL1 protein and predicted effects of mutant lesions.

Maize development can be divided into two major phases: vegetative and reproductive. During vegetative development, all non-reproductive structures are produced including leaves, roots, and stems. During reproductive development, the reproductive structures, or inflorescences, are produced. Maize makes two inflorescences, the tassel and the ear [12]. *fzt* plants have multiple vegetative and inflorescences defects, implicating miRNA regulation in multiple aspects of development. In this thesis, I investigated the roles of miRNAs during vegetative development by analyzing the vegetative phenotype of *fzt* plants. *fzt* mutant plants are considerably shorter in stature than their normal siblings. While this size difference is more prominent in the adult maize plants, it is also apparent in seedlings. The leaves of *fzt* mutant plants are also narrower and shorter than normal siblings. The difference in leaf size can be used to visually detect mutants in sibling plants only a few days old.



FIGURE 1.03. Normal and *fzt* mature maize plants
fzt (right) plants have striking phenotypic differences from normal sibling (left) plants. These differences include both inflorescence and vegetative differences.
Scale bar=12 inches

fzt mutants also have severe reproductive defects (**FIGURE 1.04**) resulting in both male (tassel) and female (ear) sterility. All meristem types in the inflorescence are less determinate than normal. Tassel florets lack glumes and produce an excess of palea/lemma type organs, resulting in a “fuzzy” appearance (B. Thompson, unpublished). *fzt* could provide a valuable tool to investigate the extensive role of miRNAs in regulating development.

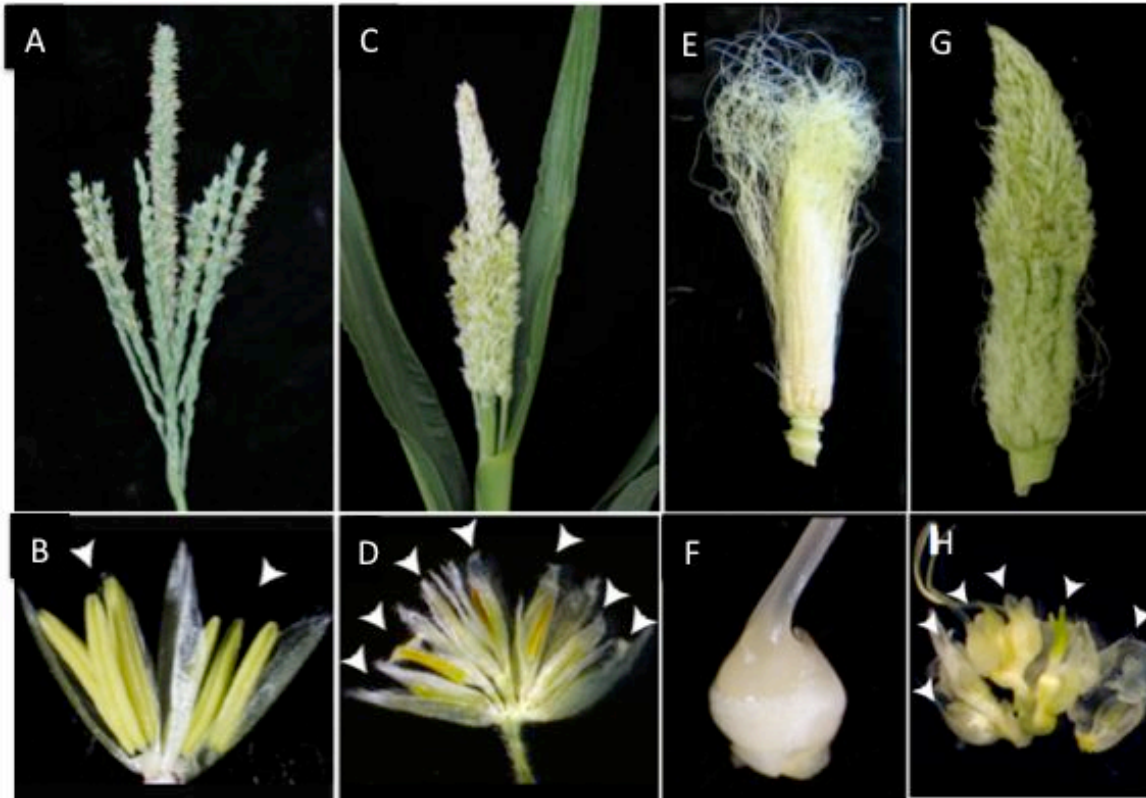


FIGURE 1.04. *fzt* Inflorescence Phenotype

A. Normal tassel. B. Normal tassel spikelet with two florets. C. *fzt* tassel. D. *fzt* tassel spikelet with seven florets. E. Normal ear. F. Normal ear spikelet with a single spikelet. G. *fzt* ear. H. *fzt* ear spikelet with six florets. Arrowheads mark florets.

Maize is an excellent model for genetic studies. Maize plants are easy to cross because they produce separate male and female parts. Furthermore, a single cross can produce ~500 seeds. The long history of maize genetics has produced an extensive collection of mutants including transposon and chemically-generated mutants. Genetic and molecular tools now make cloning of genes routine and numerous tools are available to study gene function.

Known miRNA functions in vegetative development

Leaf polarity

The maize leaf has three main axes: adaxial (top)/abaxial (bottom), proximal/distal, and medial/lateral (**FIGURE 1.05**). The proximal/distal axis refers to the distance from the point of origin, the stem. Proximal is closer to the point of origin and distal is farther from the point of origin. The medial/lateral axis refers to the distance from the middle. Medial is closer to the middle and lateral is farther from the middle. Two main surfaces of the leaf are defined as the adaxial and abaxial surfaces. The adaxial (top) surface forms closest to the main axis, the meristem, and the abaxial (bottom) surface forms farthest from the meristem. Adaxial and abaxial polarity is established in the meristem and maintained throughout organ development. This main axis of maize leaf development is regulated by several miRNAs [5, 14, 17].

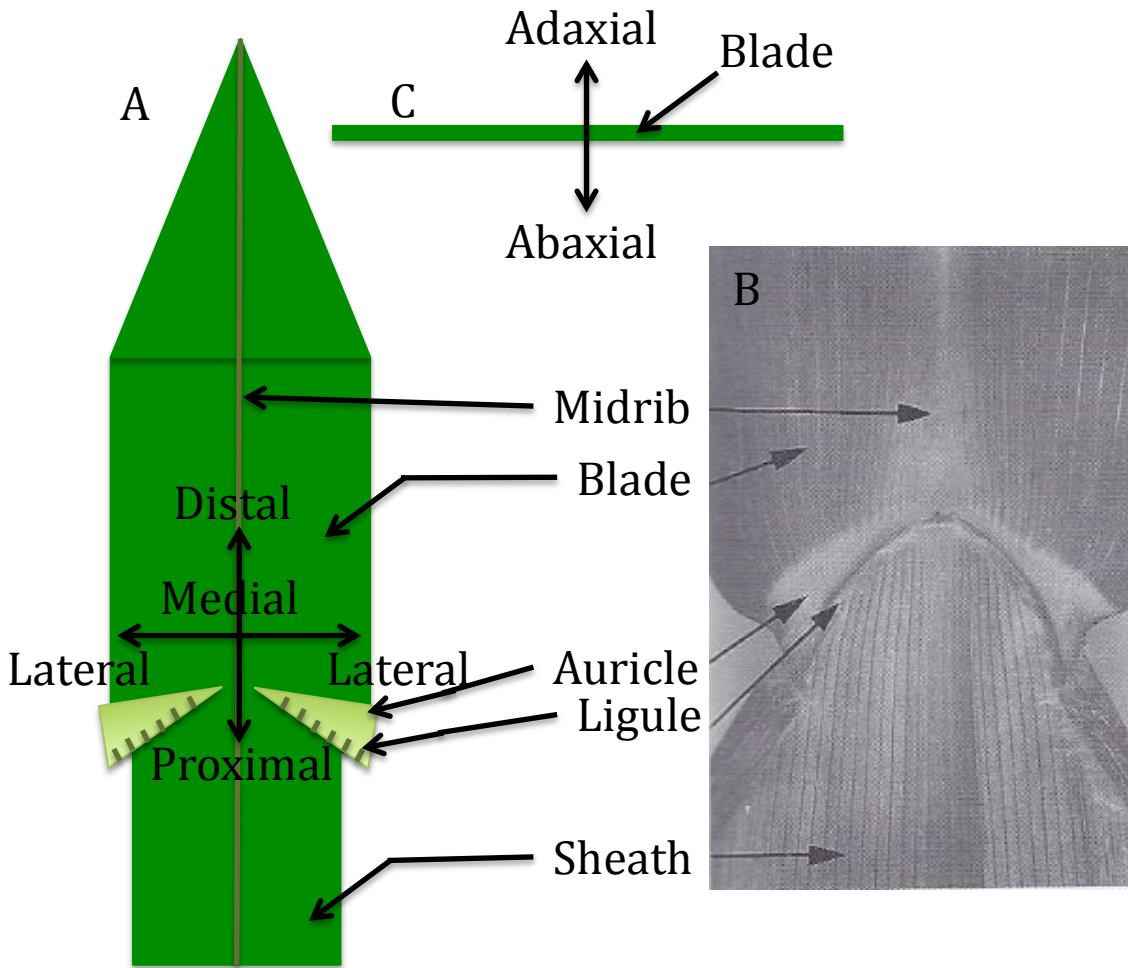


FIGURE 1.05. Leaf Axes

A. Simplified schematic of maize leaf and two commonly described axes: distal (further from the point of origin; towards tip of blade), proximal (closer to the point of origin; towards the node) and medial (towards the middle/midrib), lateral (away from the midrib). B. Adaxial surfaces of sheath, auricle, ligule, and blade maize leaf tissue. C. Simplified schematic of commonly used axis: adaxial (closest to the stem; top) and abaxial (furthest from the stem; bottom).

Several miRNAs are involved in establishing polarity in plants. miR165 and miR166 promote abaxial identity by repressing the expression of HD-ZIPIII transcription factors, adaxial

determinates that must be repressed abaxially [5, 14, 15, 17]. *Rolled leaf1 (Rld1-O)* is a dominant mutant that results in adaxialization of the blade, and results from a mutation in the miR166 binding site of the HD-ZIPIII gene, *revoluta* [14]. *Rld-O* mutant leaves are curled and the ligule tissue, an adaxial marker, is found on the abaxial surface [14], indicating the *rev* must be repressed abaxially.

miR390 is also involved in establishing leaf polarity in maize plants and acts as an adaxial determinant by repressing abaxial determinants [24]. miR390 functions in the tasiRNA pathway. Specifically, miR390 directs cleavage of the non-coding *tas3* RNA, which is then converted to dsRNA by *lbl/sgs3* and *rdr6*. The double-stranded TAS3 is processed by DCL4 into siRNA that target the ARF4 mRNA, which is specifically expressed on the abaxial surface, tasi-ARFs. The tasiR-ARFs suppress ARF4, which activates the YABBYs. The YABBYs are negatively regulated by HD-ZIPIII: *phavoluta*, *revoluta*, and *phabulosa*. The HD-ZIPIII transcription factors are adaxial determinants suppressed by miR165/miR166 [14]. The relationships between these key leaf polarity determinants are summarized in **FIGURE 1.06**.

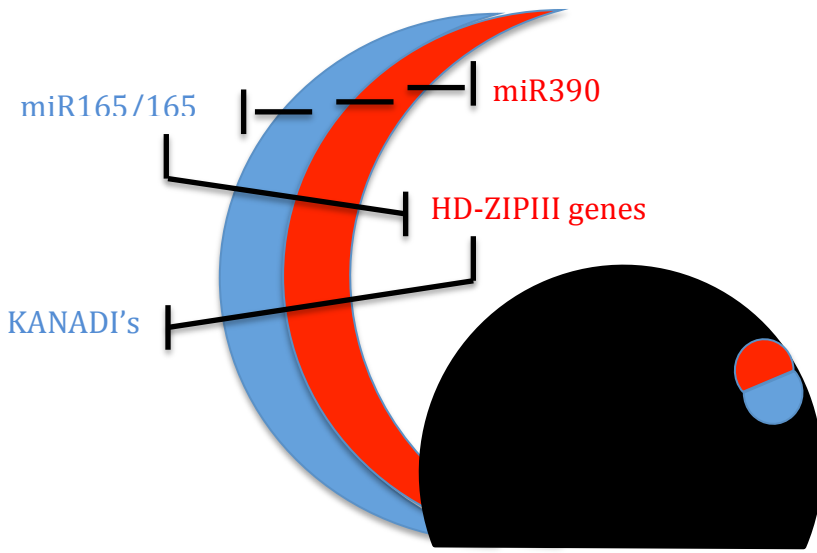


FIGURE 1.06. Proper leaf polarity is established through a network of miRNA regulation
 Several miRNAs interact in a complex network to establish proper leaf polarity, including miR390 and miR165/166 [5].

Maize leaves are composed of 4 distinct tissues: blade, auricle, ligule, and sheath. The auricle acts as a hinge to allow the blade to collect more sunlight. The ligule is the adaxial fringe around the edge of the sheath. A ring of 250 cells surrounds the shoot to form the leaf primordial [11]. Cell divisions occur early in development throughout the primordial, differentiating the leaf tissues. The pre-differentiation zone (base of blade and sheath) lacks differentiated cell types, such as stomata complexes and epidermal hairs that are present in the post-differentiation zone [13, A.J. Wright, personal communication]. Maize leaves grow from the base, meaning the oldest cells are found at the tip of the blade and the youngest are at the base [12].

The adaxial and abaxial surfaces of leaves contain distinct epidermal cell types, which can be used as polarity markers. The adaxial surface contains three different hair types: macrohairs, prickly hairs, and bicellular microhairs [20]. Macrohairs are found in organized rows of bulliform cells on adult maize leaves [25]. The macrohairs are the largest and most prominent cell type on the adaxial surface of maize leaves and are often used as adaxial fate

markers. Prickle hairs and bicellular microhairs are also found in organized rows on the adaxial surface of the leaf blade. Prickle hairs are wedge-shaped cells and do not have prominent basal cells. Prickle hairs arise from cells adjacent to veins. On the adaxial and abaxial surface of wild-type maize leaves, bicellular microhairs are present in organized rows. Bicellular hairs are the smallest hair type on the surfaces of maize leaves. The bottom half of the bicellular hair is thicker than the top half due to an unequal division. Normal maize plants do not produce prickle hairs or macrohairs on the abaxial surface [26 20, 12].

	Macrohairs	Prickle Hairs	Bicellular Hairs	Stomata
Adaxial	Yes	Yes	Yes	Yes
Abaxial	No	No	Yes	Yes

TABLE 1.01. Blade Epidermal Cell Types

Macrohairs and prickle hairs are only present on the adaxial surface of normal maize blade leaf tissue. Bicellular hairs and stomata are present on both the adaxial and the abaxial surface of normal maize blade leaf tissue.

Bulliform cells are blade adaxial epidermal cells responsible for the rolling of leaves. As the leaf loses water, the surface area is minimized to reduce sun exposure and water loss. Bulliform cells are thick, round cells. As these thick cells lose water, the cells contract and bring the margins of the blade tissue medially. In wild-type maize, bulliform cells are similar in shape to costal and intercostal long cells in that they are also rectangular in shape with the short side of the rectangle being proximal and distal to the main stem of the maize plants, but bulliform cells are considerably thicker when observed from a lateral view [2, 12, 26].

The adaxial and abaxial sheath surfaces are also distinct in normal maize plants. The adaxial surface (closest to the stem) of the sheath in wild-type maize does not contain any hairs.

This surface is composed of costal and intercostal cells, along with numerous stomata complexes. The abaxial surface (farthest from the stem) of the sheath in wild-type maize also contains costal and intercostal cells. However, there are numerous hairs present. The majority of all hair types are found between the veins of the sheath, but there are a few hairs on the periphery of the veins in wild-type maize. Compared to blade cells, sheath cells do not have specialized walls; they are straight-walled [2, 26].

	Macrohairs	Prickle Hairs	Bicellular Hairs	Stomata
Adaxial	No	No	No	Yes
Abaxial	Yes	Yes	Yes	Yes

TABLE 1.02 Sheath Epidermal Cell Types

There are no hair cells found on the adaxial surface of normal maize sheath tissue. Macrohairs, prickle hairs, and bicellular hairs are found on the abaxial surface of normal maize sheath tissue.

Vascular bundles, which consist of xylem and phloem cells, are also polarized in leaves. Xylem tissue differentiates towards the adaxial surface, whereas phloem differentiates towards the abaxial surface [10, 28].

Phase change

Phase change is another aspect of development that is regulated by miRNAs. In maize, there are several differences between adult and juvenile leaf cells including epicuticular wax composition, cell wall characteristics, and the presence of differentiated epidermal cell types such as macrohairs [21]. The juvenile traits are present in the first 4 leaves. Leaves 5 through 7 are transition leaves and exhibit a combination of juvenile and adult characteristics. Leaves 8 and older demonstrate adult characteristics in wild-type maize [6, 21].

glossy15 (gl15) controls the epidermal juvenile to adult phase change in maize in a cell-autonomous manner. *gl15* activates the expression of cell-specific juvenile epidermal wax and cell wall characteristics by suppressing the differentiation of adult epidermal cell types such as hairs [21]. Accumulation of miR172 increases during shoot development and mediates *gl15* mRNA degradation. This indicates that *gl15* maintains the juvenile phase in maize plants, and miR172 promotes the adult phase transition by down-regulation of *gl15* [17].

Corngrass1 (Cg1) maize mutant encodes two tandem miR156 genes that are overexpressed in the meristem and lateral organs [6]. These mutant plants also have lower levels of miR172. miR172 targets juvenile development genes. The overexpression of miR156 results in a prolonged juvenile development [6].

New miRNA functions in vegetative development

Leaf size

In *Arabidopsis*, cell proliferation is also regulated by miRNAs, specifically miR396. miR396 decreases cell proliferation by repressing GROWTH-REGULATING FACTOR (GRF) transcription factors in *Arabidopsis* [27]. Indeed, overexpression of miR396 reduces cell number in *Arabidopsis* leaves. miR396 is expressed at low levels in young leaves and increased during development. The balance between miR396 and *GRF* regulates cell number in leaves [27].

Clear from the examples above, miRNAs are key regulators of multiple processes in vegetative development. It is worth noting that some of these known roles of miRNAs account for some of the *fzt* phenotypes, and the cause of other aspects of the *fzt* phenotype are unknown.

My project encompasses a detailed characterization of the *fzt* vegetative phenotype. In particular, I examined the adaxial/abaxial polarity and phase change in *fzt* mutants,

based on the well-established roles of miRNAs in these processes. I also examined *fzt* mutants to implicate miRNAs in a new developmental process: organ size.

The major objectives of my project are to:

- 1) Characterize the overall vegetative *fzt* phenotype**
- 2) Characterize leaf polarity in *fzt* mutants**
- 3) Analyze mRNA Levels of HD-ZIPIII Genes**
- 4) Characterize juvenile to adult transition in *fzt* mutants**
- 5) Analyze final organ size of *fzt* leaves**

My project consists of two predominant parts: confirm perturbed vegetative phenotypes in *fzt* in regards to processes regulated by miRNAs (leaf polarity and phase change) and utilize the *fzt* phenotype to explore other developmental processes regulated by miRNAs (leaf size).

2. MATERIALS AND METHODS

GREENHOUSE PLANT PREPARATION

Seeds of families segregating *fst* were gently shaken in distilled water using a Fisher Scientific Orbital Shaker for 2 hours at 60 rpm. Seeds floating at the end of the 2 hours were considered dead, and therefore discarded. The remaining seeds were placed in 10% bleach and shaken for 15 minutes. The seeds were washed 5 times with distilled water, for 15 minutes per wash on the shaker. To prevent the growth of mold during incubation, the seeds were air dried for 3 minutes on a paper towel before applying a light coat of anti-fungal Captan. The seeds were placed embryo-side up on a wet paper towel in a glass dish. The glass dish containing the wet paper towel and Captan-treated seeds was covered with Saran wrap, secured by a rubber band, and incubated at 29°C until planted.

After 2 days in the incubator, the pericarps were removed from seeds that had not sprouted roots with forceps. After 5 days, and the appearance of shoots, the seeds were planted 4 per pot (4 ½” square pots) with Fafard potting soil and approximately 2 Tbsp. Osmocote Plus plant supplement. Before planting seeds, the soil was thoroughly soaked. Roots were completely buried in the soaked soil and the shoots were kept above the surface. Once planted, the seeds were transferred to the East Carolina University Greenhouse, where they were kept on 12-hour light cycles and greenhouse undergraduate student employees watered the pots twice daily.

When growing plants to maturity, plants were removed from the 4 ½” square pots by carefully pulling apart the four young seedlings. Plants were then transplanted to either three-gallon (1 plant/pot) or five-gallon pots (2 plants/pot). The pots were kept on 12-hour light cycles in the East Carolina Greenhouse and watered twice daily by undergraduate student employees.

GROWTH CHAMBER PLANT PREPARATION

Seeds of families segregating *fst* were prepared as previously described, but were transferred to a Percival growth chamber once planted in the 4½” pots. Thompson lab students watered the pots once daily. The growth chamber was kept at 26°C, 61% humidity, and 12 hour light cycles.

SCANNING ELECTRON MICROSCOPY (SEM)

Samples for SEM pictures were taken from blade and sheath leaf tissue. The middle of the blade was found by measuring the length of the blade along the midrib. Two samples were taken at the middle of the leaf: near the midrib and the margin. Samples near the margin included the margin hair, but did not extend more than a quarter of the total leaf width. Samples near the midrib were taken as close to the midrib as possible, but did not extend past halfway between the midrib and margin area. Sheath samples were taken between the midrib and margin hair, but did not include either.

Fresh tissue was used for all SEM pictures. Tissue collected from A619-inbred background plants was obtained from plants grown in the East Carolina Greenhouse, prepared as described above. Tissue collected from Mo17-inbred background plants was obtained from field-grown plants in summer 2011. Once harvested, all tissue was immediately kept in water to transfer to the microscope lab. In the microscope lab, tissue was measured and samples cut accordingly. Conductive Carbon Cement was used on four corners of each sample to glue samples to stubs. Glued samples were immediately placed in the SEM chamber. Samples were prepared one at a time, storing the fresh tissue in water until samples were cut.

The chamber of the FEI Quanta 200 microscope was pressurized on the low vacuum setting, with a pressure setting of 0.45 torr. The stage was centered in the chamber, and elevated

to 10 mm from the lens. The spot size was set to 3.5. The brightness and contrast were adjusted to optimize picture quality using xT Microscope Control software.

HAND SECTIONS

To examine vasculature, hand sections were made using fresh tissue from greenhouse grown plants. Fresh tissue was placed, abaxial side down, on a strip of Parafilm slightly wider than the tissue sample. The Parafilm was rolled as tightly as possible over the leaf, parallel with the main axis. The tightly wound tissue was hand cut under a Parco dissecting microscope into very thin slices using a single edge industrial razor blade. The thin slices were stained with .05% Toluidine Blue O stain for 1 minute, followed by two water rinses before mounting on a 25x75x1 mm slide in 100% glycerol.

The hand sections were observed with a BX41 microscope using dark field. Pictures were taken with an Olympus DP72 camera using the Cell Sans computer software and a 1 second exposure.

PRIMER DESIGN

Primers were designed using the Invitrogen OligoPerfect Designer (<http://tools.invitrogen.com/content.cfm?pageid=9716>). For qPCR, primers were designed to amplify ~150 bp cDNA, with a target annealing temperature of 60°C. cDNA sequences for HD-ZIPIII obtained from GenBank, accession numbers NM_001112063 (PHB) and NM_001112063 (REV).

Reference gene primer sequences were found in the literature [19].

Primer Pair Name	Forward (Sense)	Reverse (Antisense)
<i>Phabulosa</i> (CT 3/4)	5'GTTTGTGTGTGTGCGTGACA 3'	5'CTGCAACCTGCAACAGTGAT3 ,
<i>Revoluta</i> (CT 7/8)	5'GCCTTTCAATTCCCFTATGA 3'	5'ATGCCCAGCATTAGACCAG3 ,
Leunig (LUG)	5'TCCAGTGCTACAGGGAAGG T3'	5'GTTAGTTCTTGAGCCCACGC3'
Membrane Protein PB1A10.0 7c (MEP)	5'TGTACTCGGCAATGCTCTTG 3'	5'TTTGATGCTCCAGGCTTAACC 3'

TABLE 2.01. qPCR Primer Sequences

Sequences of primers used in qPCR experiments and respective abbreviations.

RNA EXTRACTION

Shoot apices, including shoot apical meristem and young leaf tissue, was collected from plants of desired age (2 weeks or 5 weeks). Leaves were removed, beginning with the oldest, one at a time. Then, the stem was cut above the prop roots. The shoot apical meristem was then dissected by cutting “up” the stem about 2/3 of total width. This allowed the SAM to be visible, and extra tissue was removed, resulting in approximately 2mm x 2mm x 3mm sample. Shoot apices were flash frozen in liquid nitrogen. Once all shoot apices were collected, snap-tubes containing the SAM tissue and liquid nitrogen were stored in an -80°C freezer until RNA extraction.

The workstation was cleaned with 95% ethanol prior to any work or collection of materials. Collected tissue was removed from the -80°C freezer and immediately put into liquid nitrogen until use. Mortars and pestles were covered in aluminum foil and baked overnight at 180°C to destroy RNases. Once cooled to room temperature, a baked mortar and pestle were used to grind collected tissue into a fine powder while adding liquid nitrogen. A liquid nitrogen-cooled scapula was used to transfer the fine powder to 1.5 mL Eppendorf tubes containing 1 mL

Tri-Reagent (Sigma). The mixture was vortexed until homogenous with as few large chunks as possible. The tubes incubated at room temperature for 8 minutes. 500 μ L of chloroform was added to the tubes and vortexed. The tubes incubated at room temperature for 2-3 minutes. Tubes were centrifuged at 4°C, maximum speed for 10 minutes. The colorless aqueous layer was transferred to new tubes with an equal volume of chloroform. Tubes were again vortexed, incubated at room temperature for 2-3 minutes, then centrifuged at 4°C, maximum speed for 10 minutes. The colorless aqueous layer was removed and transferred to new tubes with an equal volume of isopropanol and 1/10th volume of 3M sodium acetate (NaOAc). The tubes were mixed by inverting several times and incubated on ice for 20 minutes. Next, the tubes were centrifuged at 4°C, maximum speed for 10 minutes. The supernatant was discarded and the pellet was washed with 500 μ L of 70% ethanol (EtOH). The tubes incubated at room temperature for 8 minutes. The tubes were centrifuged at 4°C, maximum speed for 10 minutes. The EtOH was removed and the pellet was allowed to completely dry for 10-15 minutes. The pellet was suspended in 40 μ L DEPC water.

Following total RNA extraction, the RNA quantity was tested using a Thermo Scientific Nano Drop 2000. The reader was cleaned with DEPC water prior to any analysis and used as a blank. Concentration, 260, and 280 readings were recorded for each sample. Extracted RNA was also run on an agarose gel to visualize RNA integrity.

cDNA SYNTHESIS

The total extracted RNA was then DNase treated (New England BioLabs). The DNase treatment consisted of 5 μ L extracted RNA, 1 μ L DNase, 1 μ L 10x DNase buffer, and 2 μ L DEPC water. The reaction was incubated at 37°C for 30 minutes. Following incubation, 1 μ L 15 mM

EDTA was added. The reaction was incubated at 75°C for 10 minutes. Then, 0.7µL of 25mM MgCl₂ was added to the tubes.

DNase-treated RNA was used for cDNA synthesis using Invitrogen Superscript III First-Strand Synthesis System for RT-PCR. A 10µL reaction was prepared according to manufacturers guidelines for a final of 2µg of cDNA , with 7µL DEPC water, ~1µL total RNA, 1µL 50µM Oligo dT primer, and 1µL 10mM dNTP mix. The reaction was incubated at 65°C for 5 minutes followed by 1 minute on ice. Then, 2µL of 10x RT buffer, 4µL 25mM MgCl₂, 2µL 0.1M DTT, 1µL RNase Out (40 U/mL), and 1µL Superscript III RT (200 U/mL) was added. The 20µL reaction was incubated at 50°C for 50 minutes, followed by 85°C for 5 minutes. The tubes were chilled on ice for 3 minutes. 1µL of RNase was added before incubating the tube at 37°C for 20 minutes. Finally, 20µL of DEPC water was added to the tubes and stored at -20°C. Also, a no RT control was done every time cDNA was synthesized.

REAL-TIME PCR

Thawed cDNA, SYBRgreen (or EvaGreen), primers, and highly purified water from BBL are vortexed and centrifuged. cDNA dilutions were prepared: 1:5, 1:25, 1:125, and 1:625. 25µL reactions were prepared according to manufacturers guidelines. Plates were sealed with microseal 'B' film and loaded into the Bio-Rad CFX96 ThermoCycler.

The plate program was set to run: 95°C for 3 minutes and then cycle 95°C for 10 seconds and 59.4°C for 15 seconds (primer annealing & extension) 40 times. Lastly, a 65-95°C melt curve for 0.5 second intervals finished the real time-PCR cycle.

Standard curves and efficiency were calculated using the Bio-Rad CFX Manager Computer Software. In the software, runs are programed to calculate standard curves and efficiency for all primer sets. Wells were either categorized “Standard” or “Unknown”,

depending upon whether the well data should be used in a standard curve analysis (“Standard”) or fit to the standard curve graph (“Unknown”). If the well was to be used in a standard curve analysis, the concentrations and dilution series was also entered for each well. Data was not used in analysis if R² values were below 0.990, or if efficiency values were below 80% or above 125%.

A

Primer Set	Biological Rep 1	Biological Rep 2	Biological Rep 3
LUG	90.0%	102.1%	116.3%
MEP	98.4%	100.1%	105.9%
CT 3/4	100.1%	101.2%	125.0%
CT 7/8	97.7%	100.0%	105.9%

B

Primer Set	Biological Rep 1
LUG	87.3%
MEP	93.2%
CT 3/4	92.3%
CT 7/8	97.4%

FIGURE 2.01. qPCR efficiencies for all four experiments used in analysis

A. Calculated efficiencies for three biological replicates using 2-week old seedling tissue. B. Calculated efficiencies for one biological replicate using 5-week old plant tissue.

Once the wells were properly labeled, the “Gene Expression” tab in the CFX Manager Computer Software was used to determine fold changes between normal and *fzt* wells by calculating the ΔC_t and normalizing relative to the control. Data was analyzed relative to the control, and both reference genes were used to normalize (LUG and MEP).

GLUE IMPRESSIONS

Loctite Super Glue was applied in 5 thick strips to the surface of a microscope slide. The juvenile leaf tissue was pressed into the glue stripes, leaving some of the leaf tissue hanging off the edge of the slide. Once the tissue was pressed into the glue strips, the slide was inverted onto

a paper towel so the leaf tissue was in contact with the paper towel. A light amount of pressure was then applied to the slides with an Eppendorf rack and an empty 250 mL glass bottle. The glue was allowed to dry for 15 minutes and the leaf tissue was peeled off, using the overhang as a handle.

EPIDERMAL PEELS

A 10x fix stock solution was prepared using 20 mL 1M NaPO₄ (pH 7.2), 4 mL 0.05 M EDTA (pH 8), 0.8 g saponin, and up to 40 mL water. The pH was adjusted to 7.0. Using this 10x fix solution, a 1x fix solution was prepared fresh every time using 1 mL 10x fix, 1 mL 40% formaldehyde, and 8 mL water. A 0.05% Toluidine Blue O stain, pH 4, was used to stain the epidermal peels.

Fresh blade tissue was cut into 1 cm squares and incubated in 1x fix solution for 2 hours at room temperature. The squares were washed in water 3 times before digesting in 0.1% pectolyase for 4 hours at room temperature. The squares were washed 2 times in water. Forceps were used to peel off the epidermal layer under a dissecting microscope. The epidermal layer was stained in a drop of TBO stain for 8 minutes, and then rinsed twice in water. Peels were mounted on a glass slide in water and sealed with clear nail polish.

Epidermal peels were viewed under a Parco dissecting microscope. Pictures were taken with a Nikon camera using Nikon Image Capture computer software and a 1 second exposure and fixed aperture.

CELL SIZE MEASUREMENTS

Epidermal peels were used for cell size measurements. NIS-ELEMENTS computer software was used to detect the Toluidine Blue O-stained cell walls with a click of the mouse. The computer software measured cell area automatically using the detected cell walls and

allowed for easy and accurate manual cell length and cell width measurements. Rows of costal epidermal cells immediately adjacent to all rows of stomata were used for measurements.

CELL COUNTS

Epidermal peels were imaged and all cells in the field of view were counted. All samples were taken from the middle of the blade of leaf 8.

PROPIDIUM IODIDE STAINING

Leaf samples were stained with 0.1% propidium iodide to visualize cell walls in the pre- and post-differentiation zones. The staining was also used to visualize nuclei size differences between normal and *fzt* leaf samples.

Families known to be segregating *fzt* were grown for 2 weeks at which time leaves were measured. Leaves of about 16cm in total length were used in these studies. The basal 3 cm of the leaf blade was used as the pre-differentiation zone and the subsequent 7 cm was defined as the post-differentiation zone of interest. Once samples were cut, they were placed in 0.1% propidium iodide for 5 minutes. Once washed, the samples were mounted on a slide and viewed using an Olympus Ix81 Confocal microscope. The c-DAPI filter was used to visualize the propidium iodide. These steps were preceded by a 10-minute incubation in 40% fix solution in order to visualize the nuclei size.

TUBULIN IMMUNOFLUORESCENCE

Tissue was collected from plants when leaf 8 was visible at the minimum; to ensure only adult leaf tissue was examined. Leaves were removed one at a time, beginning with the oldest, until the leaf with an unexpanded sheath that was less than 0.5cm in length (leaf should be 20-40 cm in wild type maize) was reached. Proliferating cells (pre-differentiation zone) are found in

the basal 3 cm of this leaf. Small strips of tissue were collected from this region, as well as the post-differentiation zone (more than 3 cm from base of blade).

Collected tissue was then fixed for 2 hours while shaking in a fix solution (2.5 mL 10% formaldehyde, 10 μ L triton-X, 5 mL 2X PHEM (PIPES, HEPES, EGTA, MgSO₄, pH=7.0), and 2.5 mL BBL water). The tissue was then washed in 1X PHEM with 0.05% triton-X 3 times, while shaking, for a minimum of 30 minutes. The enzyme recipe was prepared fresh for every experiment (100 mg driselase, 50 mg pectolyase, and 10 mL BBL water). Tissue digested for exactly 15 minutes while shaking. Then, the tissue was washed 3 times in 1X PHEM with 0.05% triton-X while shaking for a minimum of 30 minutes. Tissue was then extracted for 1 hour in extraction buffer (5 mL 2X PHEM, 100 μ L DMSO, 100 μ L triton-X, and 4.8 mL BBL water) at room temperature. The tissue was washed 3 times in 1X PBS while shaking for a minimum of 30 minutes. 1X PBS with 5% normal goat serum was used to block the tissue for 30 minutes. Then, the tissue was vacuum infiltrated in the primary antibody, monoclonal Anti- α -Tubulin, (diluted in 1X PBS with 5% normal goat serum) for 30 minutes. Tissue then incubated in the primary antibody overnight at room temperature. The tissue was then washed 3 times in 1X PBS with 0.05% triton-X while shaking for a minimum of 60 minutes. Next, tissue was incubated in the secondary antibody, Alexaflor, (diluted in 1X PBS with 5% normal goat serum) for 4 hours in the dark. Tissue was then washed 3 times in 1X PBS with 0.05% triton-X while shaking in the dark for a minimum of 60 minutes, but the last wash was usually left overnight. Tissue was also stained with 10 μ g/mL propidium iodide in water for 8 minutes, washed with 1X PBS with .05% triton-X, mounted in Vectashield, and observed on the Olympus Ix81 Confocal microscope.

Antibodies were mixed 1:1 with glycerol and stored at -20°C. For use in the protocol, antibodies were diluted 1:1500 in glycerol. The Olympus Ix81 Confocal microscope was used on the “Confocal” setting using the GFP and TxRed filters.

3. RESULTS

CHARACTERIZE THE OVERALL VEGETATIVE *fzt* PHENOTYPE

To understand the broad roles of miRNAs during vegetative development, I characterized the gross *fzt* vegetative phenotype. All experiments were performed using families segregating *fzt* in the A619 inbred background. I measured internode length, root mass, and stem area using plants grown in the East Carolina University greenhouse. I measured plant height, tassel branch number, and leaf number at tassel emergence using field grown plants, grown at Central Crops Research Station in Clayton, North Carolina during the 2010 and 2011 summer field seasons. Data from both field seasons was used for analysis unless otherwise noted. Tad Herring collected the 2010 field data. No significant difference was found between field data from 2010 and 2011. For all data collection, plants were grown to maturity, as defined by tassel emergence. Student t-tests were used to determine if differences between *fzt* and normal plants were statistically significant.

Plant height

I measured the height of *fzt* and normal sibling plants (distance from the soil to the top of the main rachis of the tassel) and found that *fzt* plants were roughly 1/3 the height of normal sibling plants. Normal sibling plants averaged 163.6 cm (n=157); *fzt* mutant plants averaged 50.8 cm (n=43).

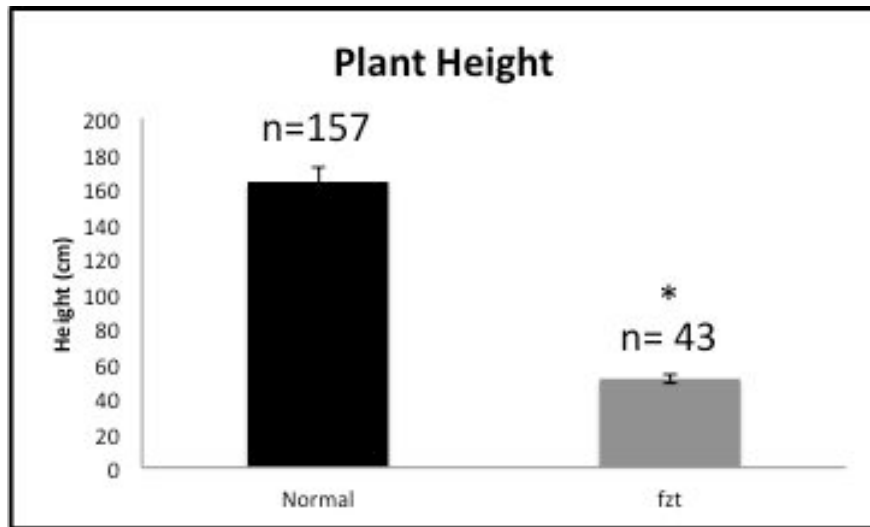


FIGURE 3.01. Plant Height

Average plant height of normal and *fzt* sibling plants. * indicates statistical significance of $p < 0.01$.

Tassel branch number

I counted the number of tassel branches in *fzt* mutant and normal sibling plants. Normal plants averaged 9.5 tassel branches (n=139), however *fzt* mutant plants made about ½ the number of branches, 5 (n=30), indicating that miRNAs likely regulate tassel branching. Tassel branch number data was only collected in summer 2011.

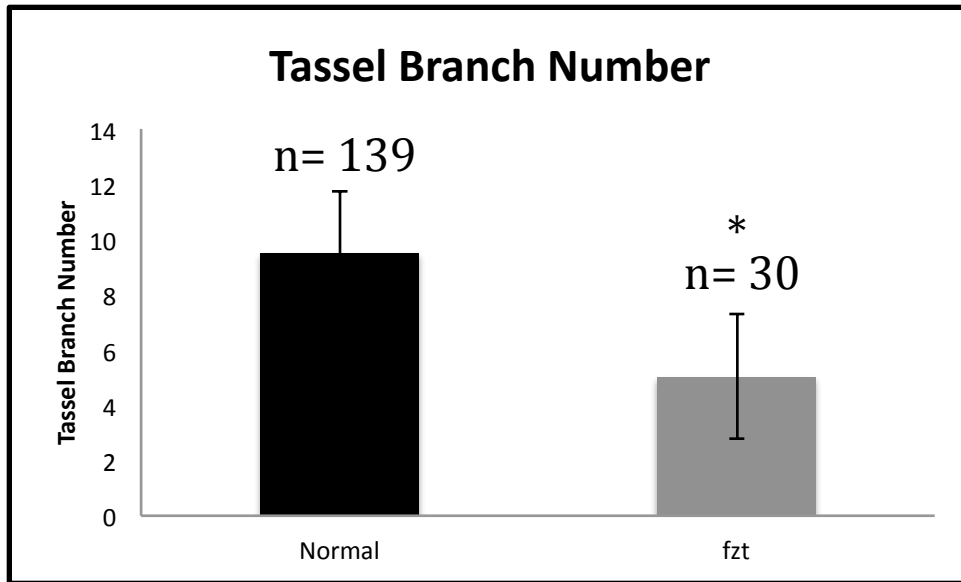


FIGURE 3.02. Tassel Branch Number

A. Average tassel branch number of normal and *fzt* sibling plants. * indicates statistical significance of $p < 0.01$. B. A *fzt* tassel (left) compared to a normal tassel. *fzt* plants make fewer, more upright tassel branches.

Leaf number

I counted the number of leaves at plant maturity (tassel emergence), and found that *fzt* plants produced about three fewer leaves than normal sibling plants. Leaves were numbered with permanent ink as they emerged, ie: the first leaf was numbered 1, the second 2, etc. because the first few leaves die as the plant continues to grow. Normal sibling plants averaged 14.8 leaves (n=157): *fzt* mutant plants averaged 11.9 leaves (n=43).

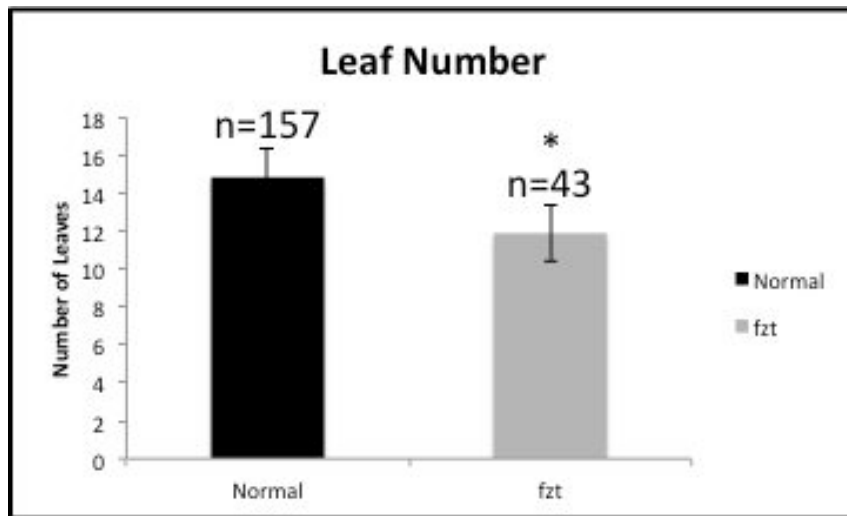


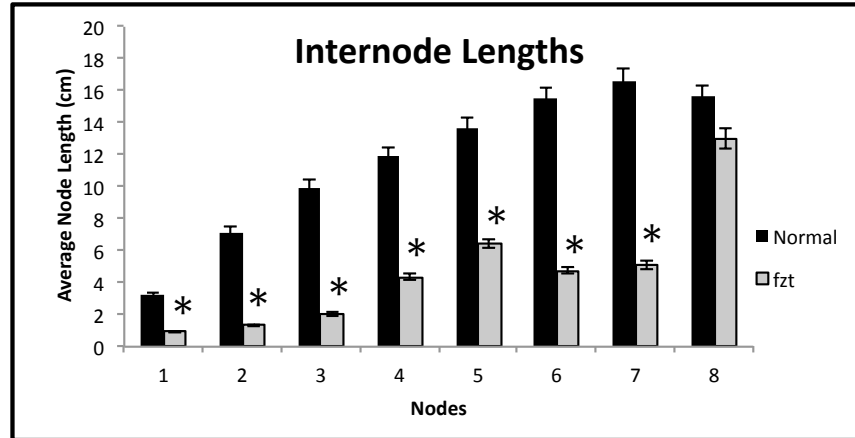
FIGURE 3.03. Leaf Number

Average leaf number of normal and *fzt* sibling plants. * indicates statistical significance of $p < 0.01$.

Internode length

Nodes are positions on the stem where a leaf inserts. Internode length is defined as the space between two consecutive nodes. Internode lengths were measured in a destructive manner, by removing the blade and sheath of all leaves, and were taken from the bottom of one node to the bottom of the subsequent node. The internodes were numbered beginning with the bottom of the stem, (1 being the first internode adjacent to the prop roots). The internode lengths of *fzt* mutant plants were significantly shorter than normal siblings for nodes 1-7, however there was no significant difference between *fzt* mutant (n=11) and normal plants (n=12) for internode 8. Figure 11 shows representatives of the first three internodes for normal and *fzt* sibling plants. Note, normal plants make more leaves and more nodes, than *fzt* plants, and therefore there is no *fzt* data for internodes 9 and beyond.

A



B



FIGURE 3.04. Internode Length

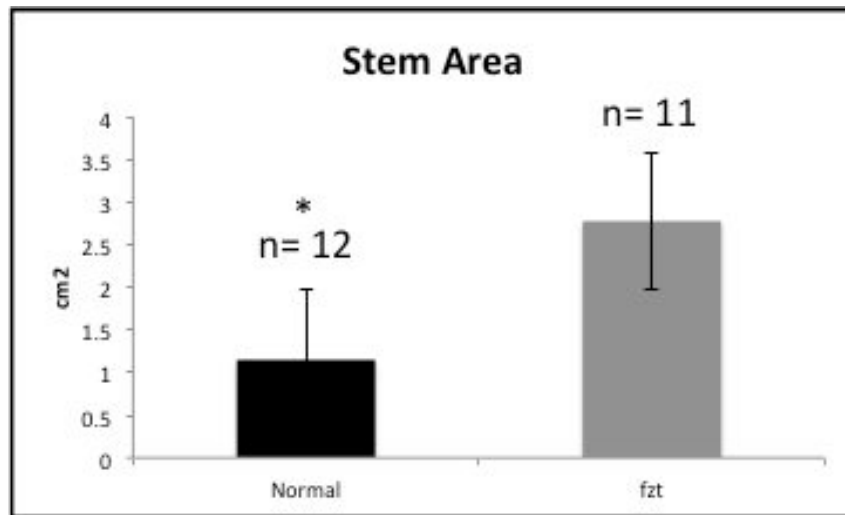
A. Average internode length of normal and *fzt* sibling plants. * indicates statistical significance of $p < 0.01$. B. A normal (left) and *fzt* plant showing the bottom four nodes. Scale bars=1 inch.

n=12 normal & 11 *fzt*.

Stem area

I calculated the stem area of *fzt* and normal sibling plants and found that *fzt* stems were larger. Stem measurements were taken at the top of the prop roots, and included both a width and length measurement of the oval. These two measurements were then used to calculate the area of the oval. Normal sibling plants averaged 1.15 cm² area (n=12): *fzt* mutant plants averaged 2.8 cm² area (n=11). These measurements were taken on greenhouse-grown plants and this phenomenon may not be observed in field-grown plants.

A



B

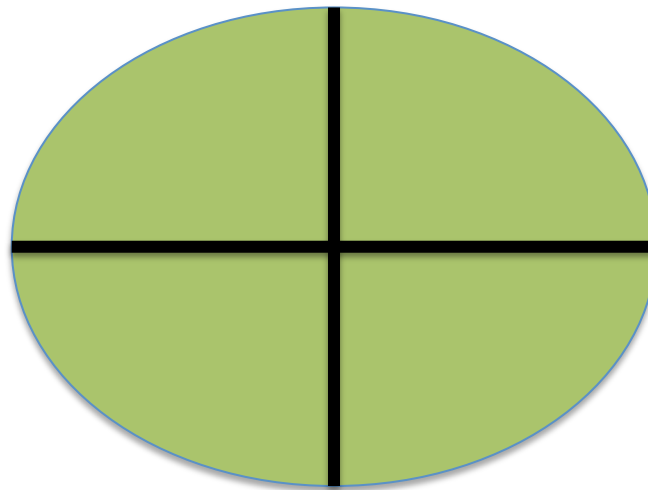


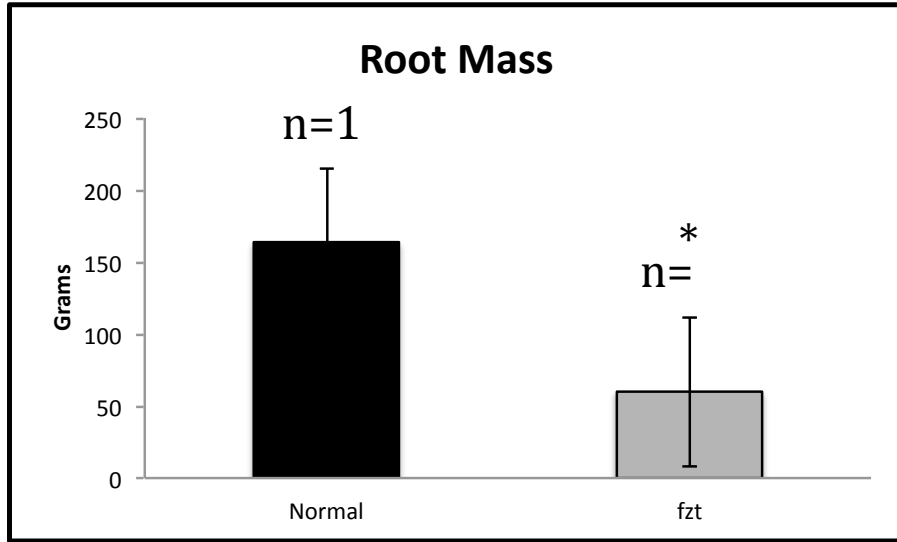
FIGURE 3.05. Stem Area

A. Average stem area of normal and *fzt* sibling plants. * indicates statistical significance of $p < 0.01$. B. Stem area was calculated by area of an oval equation ($L \times W \times 0.08$).

Root mass

I determined root mass after removing as much soil as possible with water and then allowing them to dry for 12 hours at room temperature. *fzt* plants had significantly reduced root mass compared to normal siblings. Normal sibling plants averaged 163.8g (n=12): *fzt* mutant plants averaged 60g (n=11). As seen in Figure 13, there was a visible size difference between the normal and *fzt* roots. These measurements were taken on greenhouse-grown plants and this phenomenon may not be observed in field-grown plants.

A



B



FIGURE 3.06. Root Mass

A. Average root mass of normal and *fzt* sibling plants. * indicates statistical significance of $p < 0.01$. B. A normal (left) and *fzt* root system. Scale bars=1 inch.

This general characterization of the vegetative phenotype in *fzt* mutants indicates that miRNAs have broad roles in vegetative development, including plant height, tassel branch number, leaf number, internode length, and root mass. There is little known about the specific roles of miRNAs in these developmental processes.

CHARACTERIZE ADAXIAL/ABAXIAL POLARITY

Several miRNAs establish proper leaf polarity in maize leaves, including miR390 and miR165/166 through a complex network [3, 14, 17, 23, 24]. Given the well-established role of miRNAs in establishing leaf polarity, I examined *fzt* mutants for leaf polarity defects. Unlike other mutants with perturbed leaf polarity, *fzt* has a normal ligule on the adaxial surface. To ask if *fzt* mutants had subtle leaf polarity defects, I examined epidermal cell types in blade and sheath tissue, as well as vascular polarity in *fzt* and normal sibling plants. The adaxial and abaxial surfaces of maize leaves are composed of distinct cell types. The vasculature of maize leaves orients in a specific manner: xylem towards the adaxial and phloem towards the abaxial.

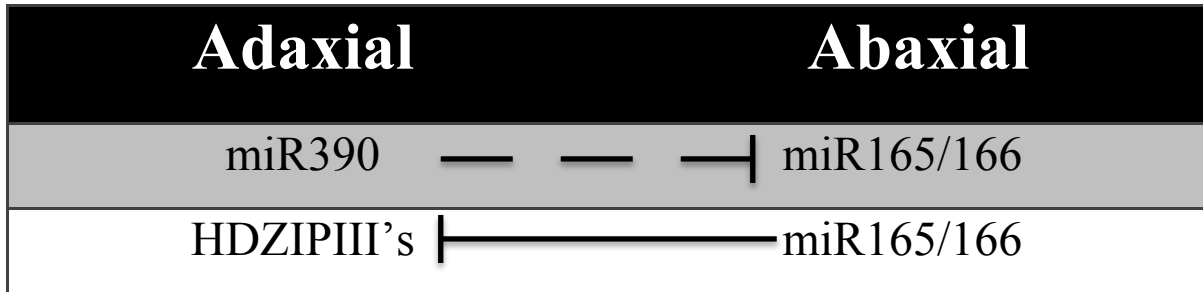


FIGURE 3.07. miRNA regulation of adaxial/abaxial polarity

Summary of miRNAs involved in establishing proper leaf polarity. miR390, an adaxial determinant, indirectly represses miR165/166, abaxial determinants. In turn, miR165/166 targets and represses the HD-ZIPIII genes [3, 5, 14, 17, 23, 24].



FIGURE 3.08. Normal Ligule Tissue

A. Side by side *fzt* (left) and normal (right) sibling adult leaves. Note the difference in length and width. B. Auricle/ligule region of the adaxial surface of *fzt* (left) and normal (right) adult leaves. The ligule (arrow) is often used as an adaxial marker. C. The auricle/ligule regions of the abaxial surface of *fzt* (left) and normal (right) sibling adult leaves. Scale bars=5 cm

Epidermal Cell Types

To determine if cell types vary depending on position of the leaf, I first examined adaxial and abaxial cell types from three regions of normal and *fzt* adult leaves: near the tip, middle, and near the base of the blade, as shown in **FIGURE 3.09**. Cell types were comparable in all three regions; I used leaf samples from the middle of the blade in all future experiments. On both surfaces, I examined cells near the margin and near the midrib, using scanning electron microscopy (SEM). Samples near the margin included the margin hair, but did not extend past a quarter of the total leaf width. The samples near the midrib began as close to the midrib as possible, but did not extend past halfway between the midrib and margin area.

	Macrohairs	Prickle Hairs	Bicellular Hairs	Stomata
Adaxial	Yes	Yes	Yes	Yes
Abaxial	No	No	Yes	Yes

TABLE 3.01. Blade Epidermal Cell Types

Epidermal cells found on specific blade tissue surfaces.

	Macrohairs	Prickle Hairs	Bicellular Hairs	Stomata
Adaxial	No	No	No	Yes
Abaxial	Yes	Yes	Yes	Yes

TABLE 3.02. Sheath Epidermal Cell Types

Epidermal cells found on specific sheath tissue surfaces.

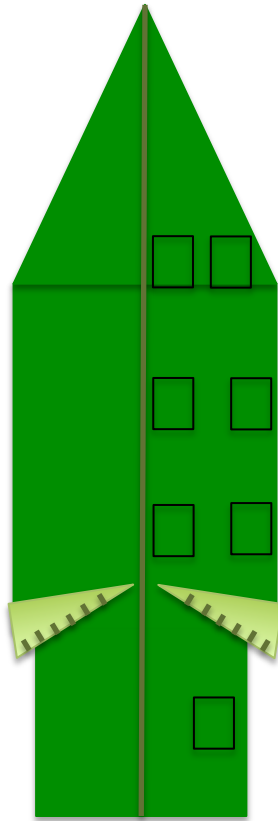


FIGURE 3.09. Leaf Sample Locations

Black boxes represent locations of samples taken for epidermal cell analysis. Due to small variation between the tip, middle, and bottom of the blade tissue, all samples were taken from the middle of the blade tissue.

To determine if adaxial and abaxial polarity is perturbed in *fzt* mutant plants, I examined adaxial and abaxial cell types in *fzt* and normal sibling plants in both the A619 background and Mo17 inbred backgrounds. The A619 specimens were backcrossed 4 times and the Mo17 specimens were backcrossed 3 times. Also, in the A619 and Mo17 background plants, samples were collected from the sheath. Both adaxial and abaxial surfaces of blade and sheath tissue were examined.

Macrohairs are often used as polarity markers because of their prominence on the adaxial leaf surface of the blade and absence on the abaxial surface [20]. In both A619 and Mo17 inbred backgrounds, I found macrohairs on the adaxial blade, and an absence on the abaxial surface in normal sibling plants. In *fzt*, macrohairs were found on the abaxial surface in both inbred backgrounds that were examined. In the A619 inbred background, macrohairs were more consistently found near the margin of leaves, but occasionally more medially on the samples. In the Mo17 inbred background, macrohairs were widely distributed across the abaxial blade. Prickle hairs are also isolated to the adaxial surface in wild type maize and were found on the abaxial surface in both inbred backgrounds. In both inbred backgrounds, there is a noticeable decrease in the abundance of macrohairs on the adaxial surface of the *fzt* mutant plants compared to a normal sibling, as seen in **FIGURES 3.10** and **3.11**. This is consistent with an abaxialization of the adaxial surface in the *fzt* mutants in the A619 background.

The stomata complexes appear to be present in similar abundance and distribution between the sibling plants, as shown in **FIGURES 3.10** and **3.11**.

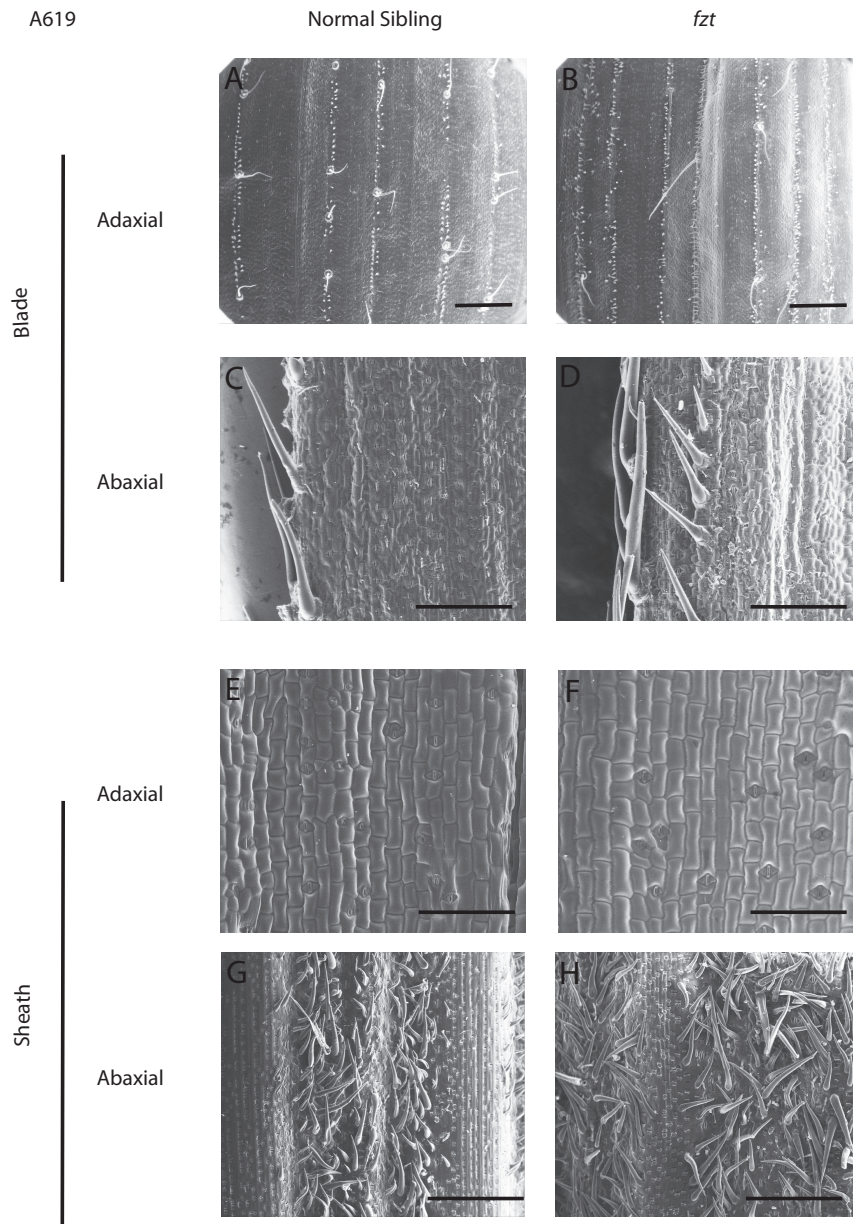


FIGURE 3.10. Epidermal cells of normal and *fzt* plants in A619 inbred background
A-D. Adaxial and abaxial blade tissue. Note the macrohairs present in (D). E-H. Adaxial and
abaxial sheath tissue. Scale bars=1 mm (A,C); 500 μm (B, D-H).

Normal Sibling

fzt

Mo17

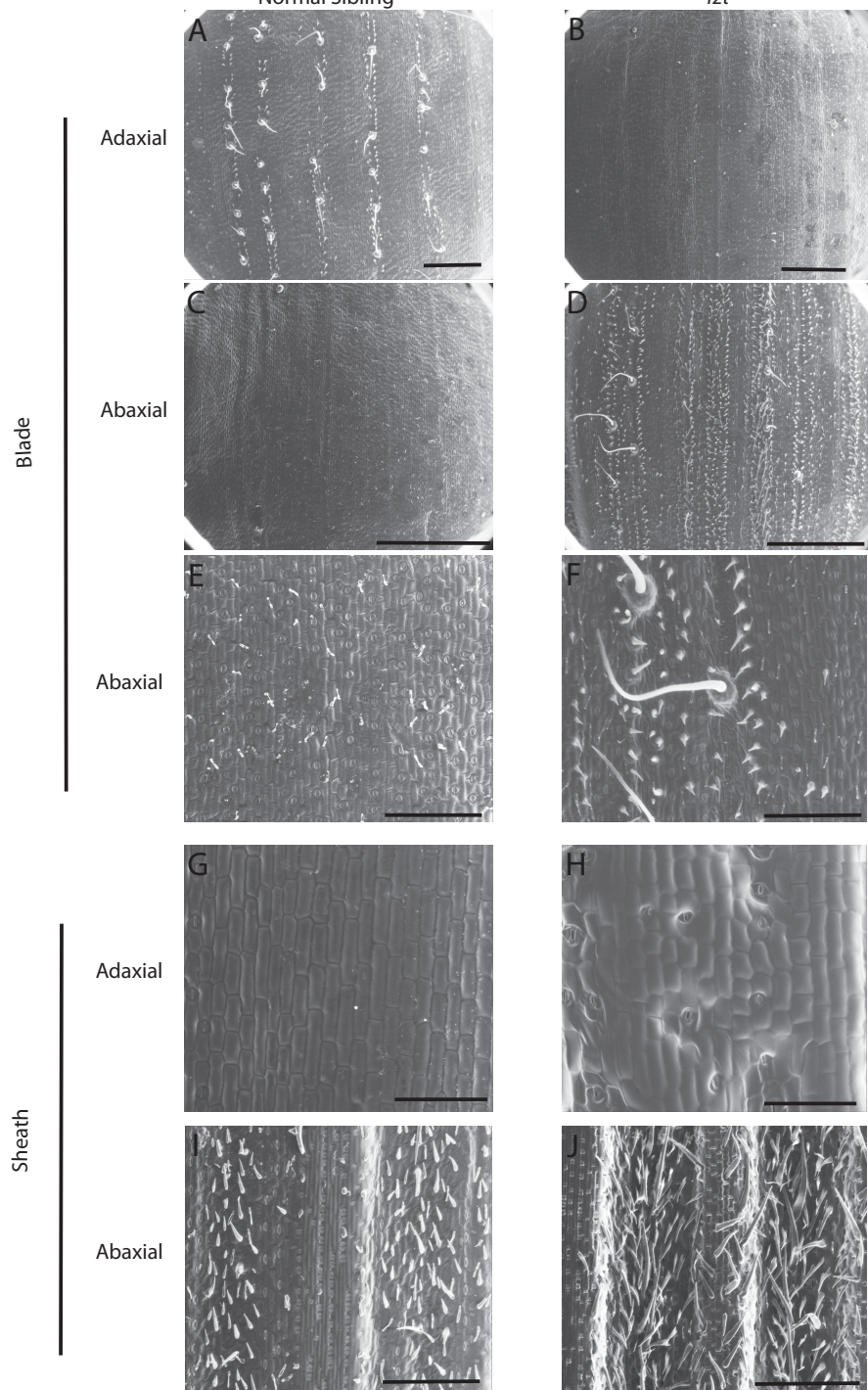


FIGURE 3.11. Epidermal cells of normal and *fzt* plants in Mo17 inbred background

A-F. Adaxial and abaxial blade tissue. Note the abundance of macrohairs in D. E and F are close-up pictures of C and D. G-J. Adaxial and abaxial sheath tissue. Scale bars=1 mm (A, C);

400 μm (B, D-J)

Vasculature Orientation

To further examine if adaxial and abaxial polarity is perturbed in *fzt* mutant plants, I examined the vasculature in *fzt* and normal sibling plants in the Mo17 background (**FIGURE 3.12**). The specimens examined were backcrossed 3 times to Mo17.

The vasculature of *fzt* mutant and normal sibling plants was compared using hand sections, very thin slices of leaf blade tissue, and stained with Toluidine Blue O. I examined 4 normal and 4 *fzt* plants. In wild type maize, xylem orients towards the adaxial surface and phloem orients towards the abaxial surface. Indeed, in normal siblings I observed xylem oriented towards the adaxial surface, and phloem oriented towards the abaxial surface. In *fzt* plants, leaves 4, 5, 6, and 7 were indistinguishable from normal siblings, however I observed a subtle polarity defect in leaves 8, 9, and 10. In ~25% of the vascular bundles from leaves 8 and 9, xylem cells extended more abaxially and I observed this same polarity defect in ~50% of vascular bundles in leaf 10 of *fzt* mutant plants.

Mo17 Hand Sections

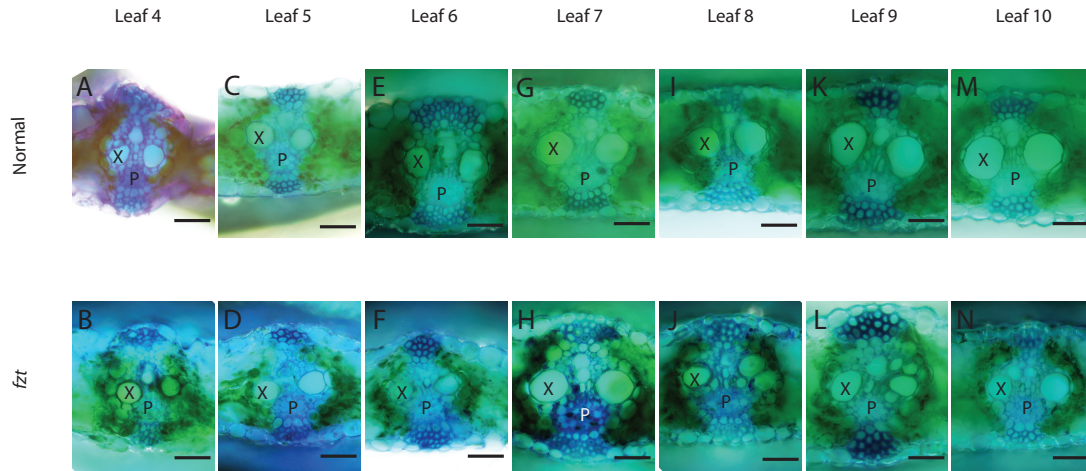


FIGURE 3.12. Vasculature orientation of normal and *fzt* plants in Mo17 inbred background
 A-B. Juvenile leaf vascular orientation of normal (A) and *fzt* (B). C-H. Transition leaf vascular orientation. I-N. Adult leaf vascular orientation. Note the xylem (X) cells of *fzt* leaves.

X=xylem, P=phloem, Scale bars=50 μ m.

mRNA LEVELS

miRNAs, specifically miR165 and miR166, negatively regulate the expression of the HD-ZIPIII genes, which promote adaxial fate [14]. I expect to see an increase in the mRNA of miRNA target, if miRNAs are reduced in *fzt*. Therefore, using quantitative RT-PCR, I examined the expression of two HD-ZIPIII genes.

Total RNA was extracted from shoot apices from 2-week old normal sibling and *fzt* plants and used for cDNA synthesis (three biological replicates). The extracted RNA was used to analyze mRNA levels of two HD-ZIP III genes: *revoluta* and *phabulosa*.

Surprisingly, I did not see altered mRNA levels in *fzt* mutant plants. All replicates had very small fold change differences in mRNA levels between *fzt* and normal sibling plants: less than 1.5-fold difference.

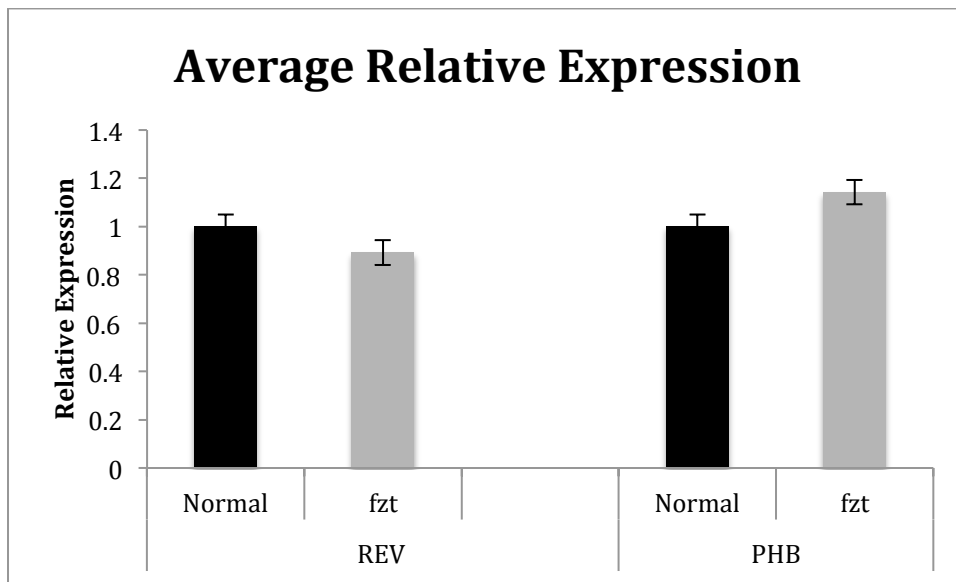


FIGURE 3.13. Gene expression data for three biological replicates of 2-week old seedlings. Gene expression data normalized to both LUG and MEP. All calculations were normalized relative to control. No significant difference was found between *fzt* and normal sibling plants.

I further explored the mRNA levels of the HD-ZIPIII genes using shoot apices from 5-week old normal and *fzt* plants. Consistently, I found the vegetative *fzt* phenotype more severe as the plant matures.

However, the mRNA levels of *revoluta* and *phabulosa* in the 5-week plant tissue, similar to those of the juvenile seedlings, had very little difference in mRNA levels between normal and *fzt* mutant plants. In the one biological replicate, there was less than a 1-fold change for both target mRNAs.

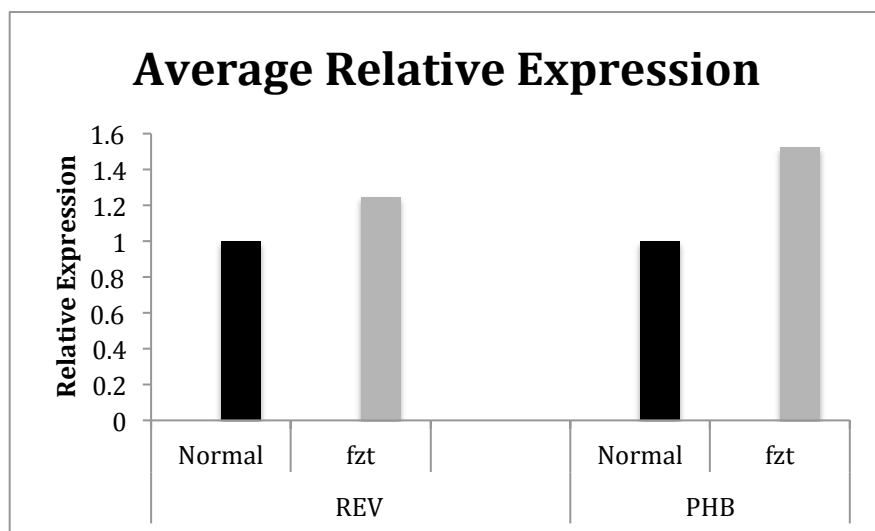


FIGURE 3.14. Gene expression data for one biological replicate of 5-week old plants

Gene expression data normalized to both LUG and MEP. All calculations were normalized relative to control. No significant difference was found between *fzt* and normal sibling plants.

CHARACTERIZE JUVENILE TO ADULT TRANSITION

Phase change is controlled by the antagonistic activities of two miRNAs. miR156 promotes juvenile fates and miR172 promotes adult fates. *Corngrass1 (Cg1)*, a maize mutant in which miR156 is overexpressed, significantly extends the juvenile phase, in part by reducing miR172 levels [6, 7]. If *fzt* has altered levels of miR156 and/or 172, we would expect phase change to be altered in *fzt* plants compared to normal siblings. Therefore, I examined phase change in both *fzt* and normal plants in both the A619 and Mo17 inbred backgrounds.

Maize juvenile and adult leaves differ in several traits including epicuticular wax composition, cell wall characteristics, and the presence of differentiated epidermal cell types such as macrohairs [21]. Juvenile leaf traits are present in the first 4 leaves, leaves 5 through 7 are transition leaves exhibiting both juvenile and adult characteristics, and leaves 8 and older demonstrate adult characteristics in wild-type maize [21].

Adult and juvenile maize leaves produce different epicuticular waxes, which are produced cell autonomously. Juvenile leaves produce a dull blue wax full of fatty alcohols. Adult leaves produce a wax of wax esters. Juvenile waxes will stain violet and adult waxes will stain blue/aqua with Toluidine Blue O (**TABLE 3.03**).

Trait	Juvenile	Adult
Epidermal Hairs	Absent	Present
Bulliform Cells	Absent	Present
Cell Shape (Cross-Section)	Rounded	Rectangular
Cell Wall Invagination	Moderate	Extreme
Epicuticular Waxes	Dull Blue, Fatty Alcohols	Reduced Levels, Was Esters
Toluidine Blue O Staining	Purple	Blue

TABLE 3.03. Juvenile and Adult Leaf Cell Characteristics

List of characteristics specific to juvenile and adult leaves that can be used to differentiate leaf stages.

To examine the juvenile to adult transition in *fzt* plants, I examined leaf waxes of leaves 4 through 8 from *fzt* mutant and A619 plants. I first looked at leaves 4 and 8, but saw no difference between normal and *fzt* mutant plants, indicating no major defect in phase change. To determine if there is a subtle defect, I looked at the transition leaves, 5 through 7.

As seen in **FIGURE 3.15**, *fzt* mutants begin producing adult epicuticular waxes on the adaxial surface approximately one leaf earlier than normal sibling plants. In the A619 inbred background, normal plants began producing adult waxes at leaf 7 and *fzt* mutant plants began producing adult waxes at leaf 6.

A619 Epidermal Peels

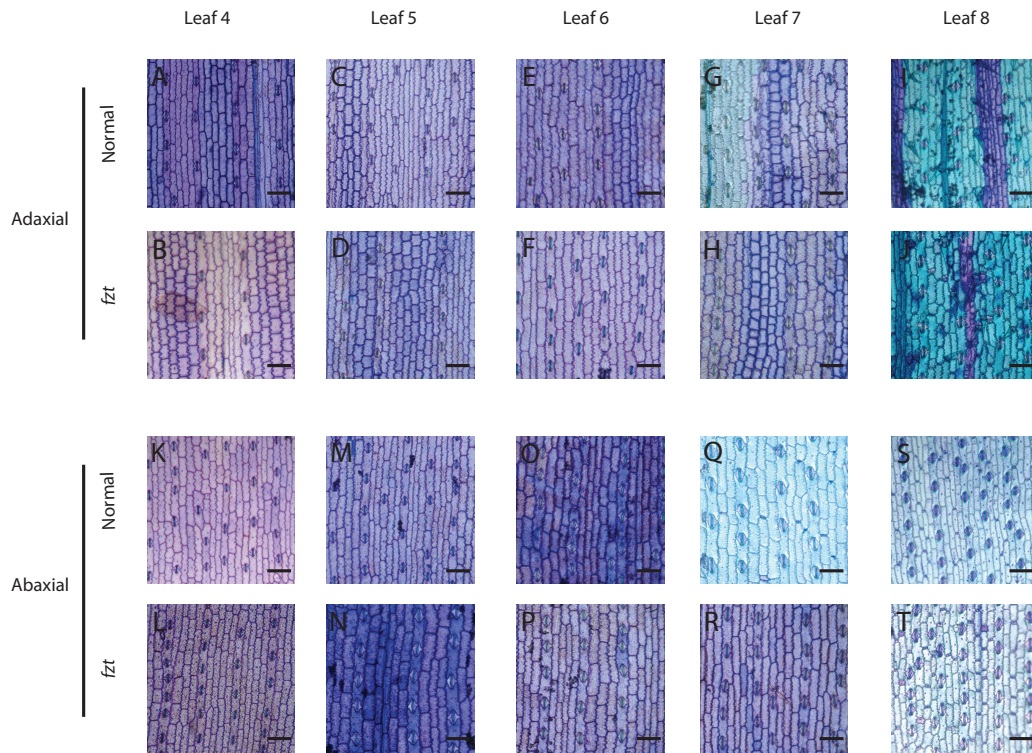


FIGURE 3.15. A619 Epidermal Peels

A-J. Adaxial surfaces of normal and *fzt* plants. Note the difference in staining at leaf 7. K-T.

Abaxial surfaces of normal and *fzt* plants. Note the difference in staining at leaf 7.

Scale bars=100 μ m

In the Mo17 inbred background, normal plants began producing adult waxes at leaf 6 and *fzt* mutant plants began producing adult waxes at leaf 5. *fzt* mutant plants stained a combination of purple and blue, indicative of juvenile and adult waxes. The perturbed epicuticular wax pattern of the *fzt* plants was observed in about 1/3 of all samples, and was concentrated around the vasculature of the peels. This subtle phase change difference is consistent with the known role of miRNAs in establishing proper juvenile to adult transition in maize plants.

Mo17 Epidermal Peels

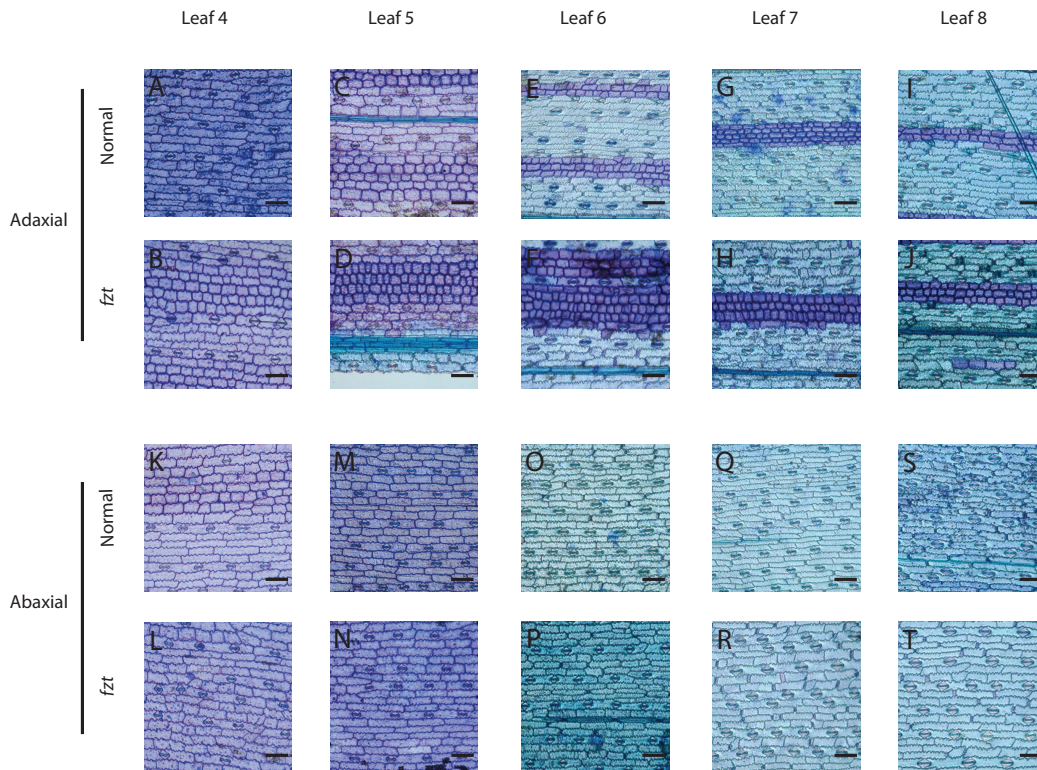


FIGURE 3.16. Mo17 Epidermal Peels

A-J. Adaxial surfaces of normal and *fzt* plants. Note the early onset of blue staining in *fzt* at leaf

5. K-T. Abaxial surfaces of normal and *fzt* plants. Note the similar staining at all leaves.

Scale bars=100 μ m

The adult leaf samples stained in a similar fashion between the normal and *fzt* mutant plants. Adaxial samples stained a bright blue color with rows of bright purple bulliform cells. However, subtle differences were observed on the abaxial surfaces. The *fzt* mutant plants displayed larger silica cells at the base of the bicellular hairs on the abaxial surface compared to normal siblings.

Also worth noting, there was a difference in the organization of the cell rows between *fzt* mutant and normal plants. Epidermal cells were organized in continuous rows of cells approximately the same size in normal plants while the *fzt* epidermal cells varied more in size and organization, with some cell rows merging into a single row of cells. There also appeared to be a difference in the number and distance between bulliform cell rows.

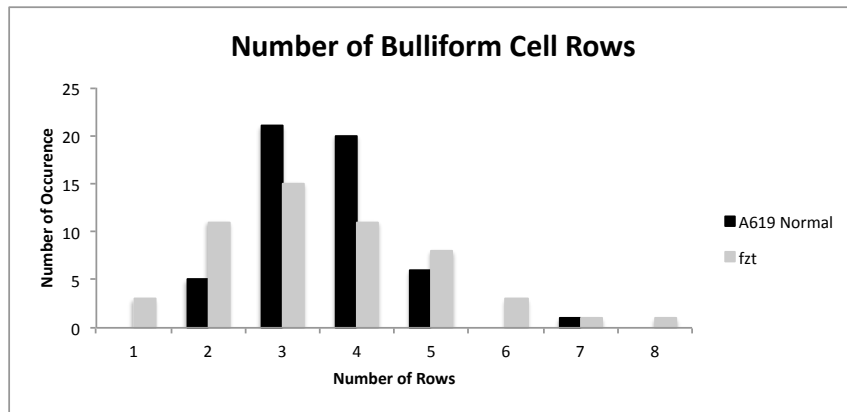


FIGURE 3.17. A619 Bulliform Rows

Distribution of the number of bulliform cell rows in *fzt* and normal sibling plants. Most normal plants had 3-4 rows of bulliform cells, however *fzt* plants had more variation in the number of bulliform cells.

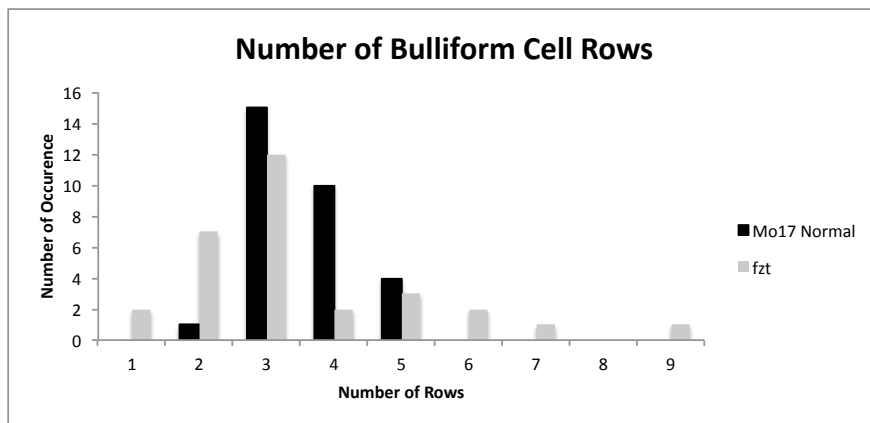


FIGURE 3.18. Mo17 Bulliform Rows

Distribution of the number of bulliform cell rows in *fzt* and normal sibling plants. *fzt* had a wider variety of bulliform rows compared to normal siblings.

ANALYZE LEAF CELL SIZE AND NUMBER

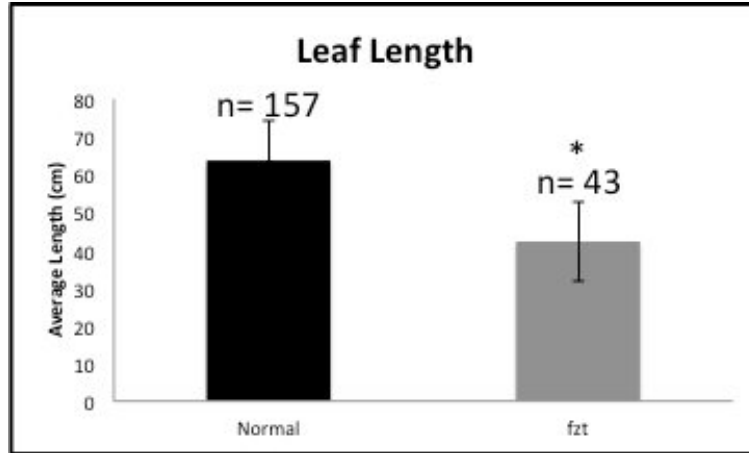
Cell size, cell number, or a combination of the two determines final organ size in plants. *fzt* mutant plants are shorter in stature and have shorter, narrower leaves than normal siblings, suggesting that miRNAs have a role in regulating cell size and/or cell proliferation. This is one aspect of vegetative development in which *fzt* could expound on our working knowledge of miRNAs and their role in plant development.

Overall Leaf Size

Preliminary data established that *fzt* leaves are shorter and narrower than normal siblings (B. Thompson, unpublished). I repeated these measurements for the 2011 field season using leaf 9 of A619 background field-grown plants. The length measurements were taken from the tip of the leaf to the bottom of the blade along the midrib. Width measurements were taken at the middle of the leaf blade from margin to margin. The blade tip was folded to touch the auricle tissue to determine the middle of the blade. This data was then compared to field data collected in summer 2010.

I found statistical difference between both leaf length and width between the normal and *fzt* sibling plants. Normal plants averaged 63.73 cm in length, while *fzt* averaged only 42.27 cm in length. A greater difference was seen in the leaf width averages between normal (7.88 cm) and *fzt* (3.39 cm).

A



B

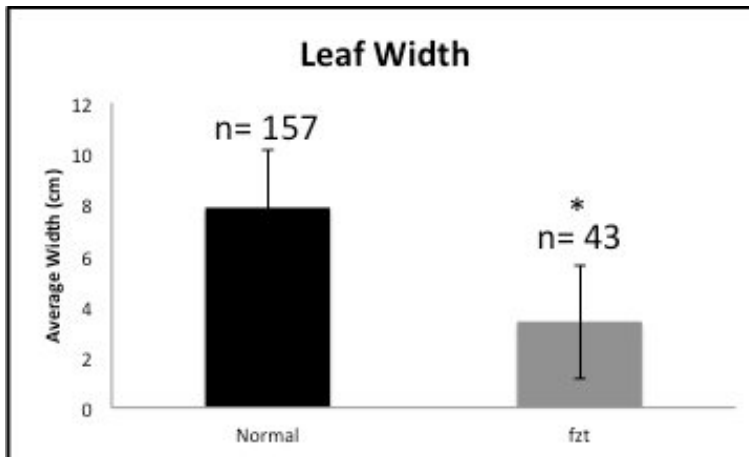


FIGURE 3.19. Leaf Length & Width Differences

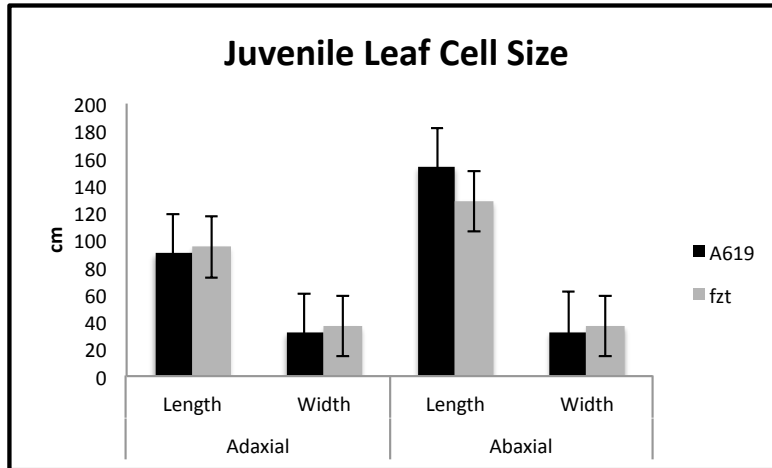
A. Leaf length measurements of *fzt* and normal sibling plants. B. Leaf width measurements of *fzt* and normal sibling plants. All measurements were taken on plants in A619 inbred background.

* indicates statistical significance ($p < 0.01$).

Cell Size

To determine if the decrease in overall leaf size was caused by a decrease in cell number or a decrease in cell size, I first measured cell length, width and area of the cells immediately adjacent to all rows of stomata. The juvenile leaves did not demonstrate a significant difference in the length, width, or cell area between the *fzt* and normal sibling plants, as seen in **FIGURE 3.20**. There is a subtle difference in leaf size in juvenile leaves, and therefore I did not expect a large difference in cell size in juvenile leaves, even if cell size is a higher contributor to the decrease in final leaf size.

A



B

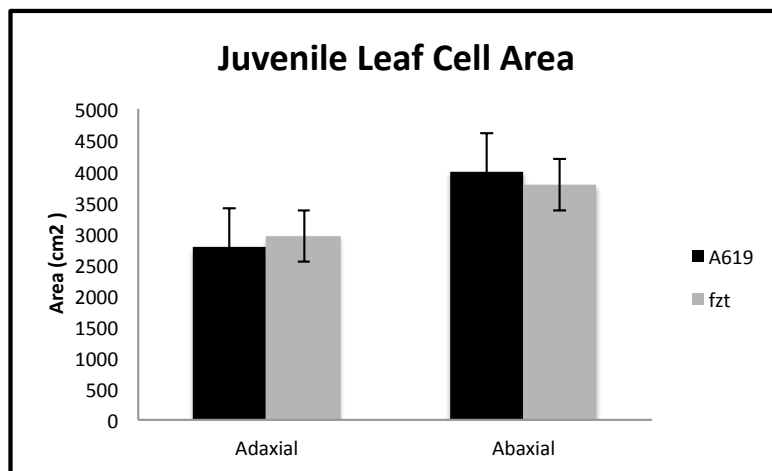


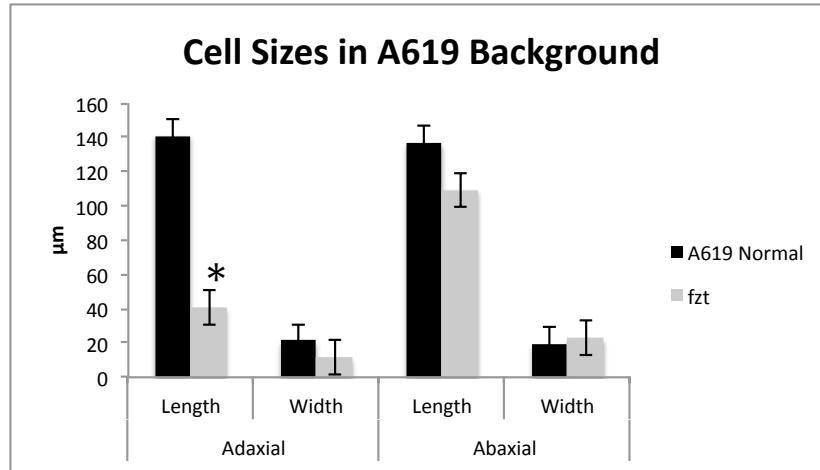
FIGURE 3.20. Juvenile Leaf Measurements

A. Cell length and width measurements of A619 and *fzt* plants. B. Cell area measurements of A619 and *fzt* plants. All measurements were taken at the middle of leaf 4.

B. n=4 A619 and n=4 *fzt* plants.

These measurements were repeated using adult leaves, where the difference in final organ size appears to be greater. Surprisingly, there was no statistical difference in cell length, width, or area measurements between *fmt* and normal sibling adult leaves (**FIGURE 3.21**).

A



B

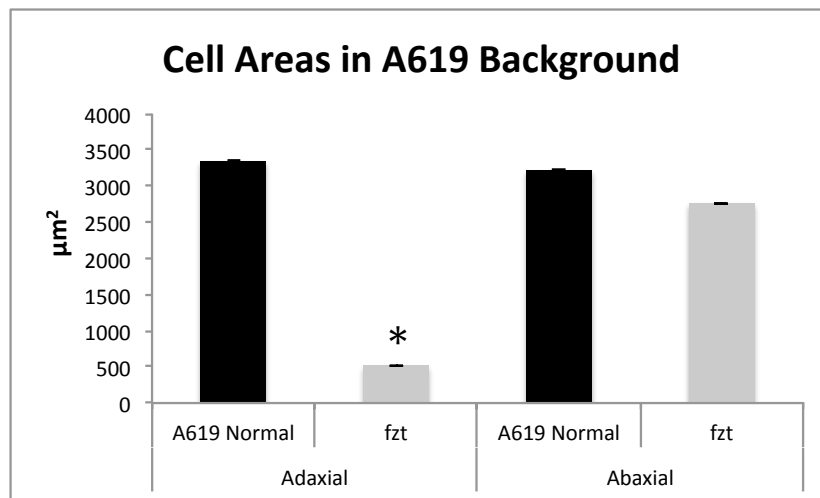
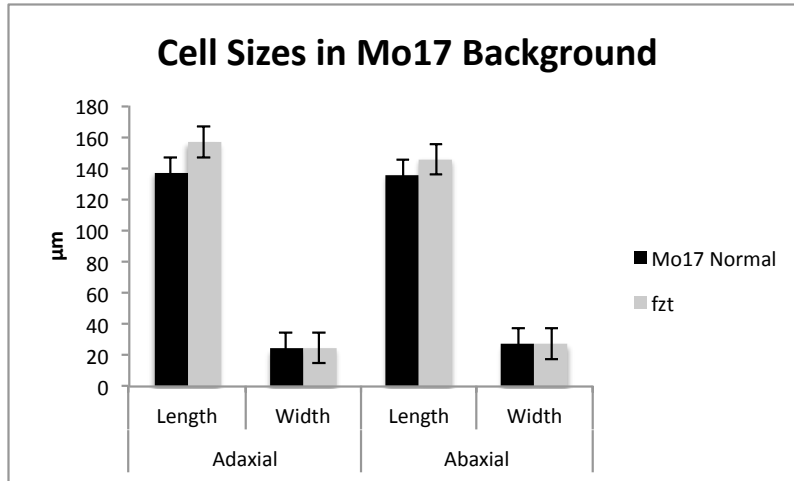


FIGURE 3.21. A619 Adult Cell Size Measurements

A. Cell length and width measurements of normal and *fzt* plants. B. Cell area measurements of normal and *fzt* plants. All measurements were taken at the middle of leaf 8.

B. n=8 normal sibling and n=8 *fzt* plants.

A



B

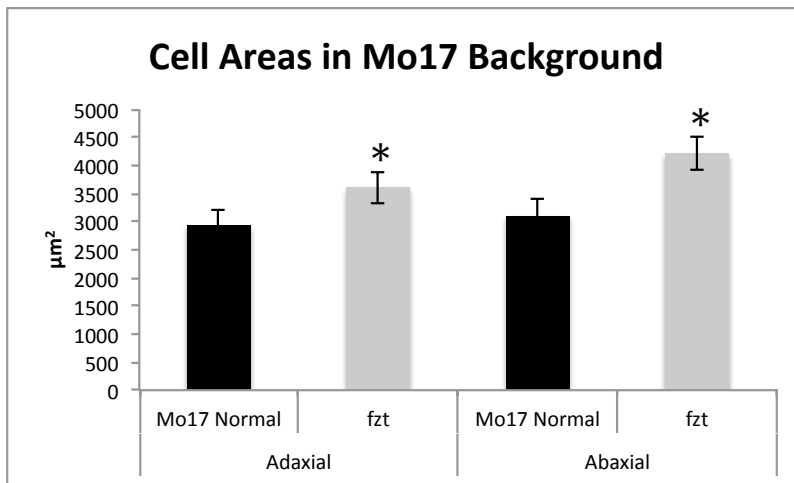


FIGURE 3.22. Mo17 Cell Size Measurements

A. Cell length and width measurements of normal and *fzt* plants. B. Cell area measurements of normal and *fzt* plants. All measurements were taken at the middle of leaf 8.

n=4 normal sibling and n=4 *fzt* plants.

Because the row of cells beneath the stomata might not be representative of cell size throughout the tissue (and cell size in *fzt* plants was more variable than in normal siblings), I also counted the total number of cells within a unit area. If the reduced leaf size in *fzt* plants is due to a decrease in cell size, then I would expect to observe more cells within a given unit area in *fzt* plants than in normal plants. If, however the reduced leaf size is due to a decrease in cell number, I would expect to observe the same number of cells within a given unit area in *fzt* and normal plants. Finally, a reduced leaf size could be due to a combination of reduced cell size and cell number, in which case I would expect to observe a difference in both the cell size and cell number between normal and *fzt* plants.

Collectively, this data provides insight into a potentially new role of miRNAs in vegetative development.

4. DISCUSSION

miRNAs

miRNAs are short (~22 nt) non-coding RNAs that regulate diverse processes in both plants and animals including normal development, carcinogenesis, and stress responses [4,16, 30]. In plants, miRNAs regulate multiple developmental processes including leaf polarity, phase change, and inflorescence development [3, 6, 7, 8, 15, 17, 23, 24]. In the work described here, I analyzed vegetative development in the maize *fuzzy tassel (fzt)* mutant. *fzt* contains a mutation in DICER-LIKE1, a key enzyme required for miRNA biogenesis and *fzt* phenotypes are likely due to reduced miRNA levels (B. Thompson & B Meyers, unpublished). To characterize the *fzt* mutant, I both examined vegetative processes known to be regulated by miRNAs in maize (leaf polarity and phase change) and processes for which miRNA regulation is currently unknown (organ size). This work gives insight into the nature of the *fzt* mutant, as well as implicates miRNAs in new aspects of development.

Leaf polarity and phase change are two vegetative development processes in which the roles of miRNAs have been extensively studied. Therefore, I began by looking at these processes first. These experiments confirmed that *fzt* have defects in miRNA regulated processes, consistent with a mutation in *dcl1*. Interestingly, *fzt* plants had subtle phase change and leaf polarity defects, indicating that the levels of miRNAs and/or miRNA targets important for these processes are not drastically altered in *fzt* mutants.

***fzt* HAS DEFECTS IN KNOWN miRNA REGULATED PROCESSES**

Leaves have three developmental axes: proximal/distal, medial/lateral, and adaxial (top)/abaxial (bottom). The adaxial/abaxial axis is controlled by a complex regulatory network that involves multiple small RNAs, including miRNAs [5, 14, 17].

Given the well-established role of miRNAs in determining adaxial/abaxial polarity, we examined *fzt* mutant plants for polarity defects. In other mutants with perturbed adaxial/abaxial polarity, such as *Rolled-1 (Rld-1)*, the ligule tissue, which is normally only found on the adaxial surface, is also found on the abaxial surface [14, 15, 22]. The ligule was positioned normally in *fzt* mutant plants, indicating that there were no gross polarity defects. However, I found that *fzt* mutant plants had subtle leaf polarity defect, consistent with perturbed miRNA levels.

The adaxial and abaxial surfaces of maize leaves are composed of distinct cell types. Macrohairs are often used as polarity markers because of their prominence on the blade adaxial surface [2, 20, 22]. In *fzt*, macrohairs were present on the abaxial surface in both the A619 and Mo17 inbred backgrounds. This is consistent with an adaxilization of the abaxial surface. Also, we saw fewer macrohairs on the adaxial surface of *fzt* mutants compared to normal siblings, consistent with an abaxilization of the adaxial surface.

Leaf vasculature is also polarized along the adaxial/abaxial axis. Xylem is oriented towards the adaxial surface and phloem is oriented towards the abaxial surface [10, 28]. I also asked if vascular was perturbed in *fzt* plants. Indeed, I found that the xylem were located more abaxially in adult leaves (8-10) of *fzt* mutant plants. Also, vascular bundles were less organized in *fzt* mutants compared to normal siblings in that xylem cells were smaller and more scattered within the bundle in adult leaves. Interestingly, the vascular phenotype increased in severity after the plant transitioned to adult leaves. This could be caused by an increase in the altered mRNA levels in mature plants versus juvenile plants. If this is the case, *fzt* plants should be analyzed for miRNAs that regulate development in juvenile leaves but not in adult leaves and vice versa. These analyses could explain the increase in severity of *fzt* as the plants mature.

Together, these experiments indicate that *fzt* mutants have defects in establishing adaxial/abaxial polarity, consistent with decreased miRNA levels. The miRNAs, miR165 and miR166, negatively regulate expression of three HD-ZIPIII genes, which promote adaxial fate. If miRNAs are reduced in *fzt*, I expected to see an increase in the mRNA of miRNA targets. Therefore, I examined the expression of two of these HD-ZIPIII genes using quantitative RT-PCR. Surprisingly, there was little difference in HD-ZIPIII expression between normal and *fzt* plants at both the 2-week and 5-week stages.

There are several explanations that could account for the lack of mRNA difference between *fzt* and normal siblings. Shoot apical meristem and young leaf tissue was collected for this analysis, which may not be representative of differing mRNA levels in the overall leaf, where we see the perturbed polarity. Another explanation could be the number of affected cells is averaged out in the collected tissue. mRNA levels of the HD-ZIPIIIs may be affected in a few cells, and the change in these few cells are averaged out with the less-affected cells that were also collected for these experiments.

Future experiments should be carried out in order to test the mRNA targets of other miRNAs shown to regulate vegetative development.

To further characterize the perturbed leaf polarity phenotype of *fzt* maize mutant, in situ hybridization experiments could be used to visualize the location of the mRNA targets of specific miRNAs, such as the HD-ZIP III genes. If these miRNA targets are found to be mislocated, that could assist in explaining the perturbed leaf polarity we see in *fzt*.

The juvenile to adult transition, or phase change, is also regulated by miRNAs. Overexpression of miR156, as seen in *Corngrass1 (Cg1)*, results in overexpression of juvenile traits. *Cg1* was also found to have decreased levels of miR172 [6]. miR172 promotes the adult transition by targeting genes, such as *glossy15 (gl15)*, that control juvenile traits [17]. Given the well-established role of miRNAs in determining proper juvenile to adult transition, we examined *fzt* mutant plants for perturbed phase change.

There are several aspects of development to differentiate between juvenile and adult characteristics, such as the epicuticular waxes. The epicuticular waxes are produced cell-autonomously and differ in composition between juvenile and adult leaves. When stained with Toluidine Blue O, juvenile waxes stain a purple and adult waxes stain bright blue [9, 21]. In both the A619 and Mo17 backgrounds, we saw an early onset of adult characteristics in the *fzt* mutant plants, about one leaf early compared to the normal sibling plants.

There are several explanations that could account for the lack of juvenile to adult transitional timing difference between *fzt* and normal siblings. One explanation could be the miRNA levels are not drastically affected in *fzt*, resulting in subtle vegetative differences. Also, opposing activities of two miRNAs regulates phase change, and if both of these miRNA levels are lowered, that could result in subtle transition differences in the *fzt* mutant compared to normal plants.

***fzt* HAS DEFECTS IN UNKNOWN miRNA REGULATED PROCESSES**

A general characterization of the vegetative phenotype quantified various aspects of the *fzt* mutant that are uncharacteristic of the normal phenotype, and highlighted significant differences between the two distinct phenotypes, such as plant height, tassel branch number, and leaf number. We also found significant differences between *fzt*

mutants and normal siblings in regards to internode length, stem area, and root mass, however these measurements were taken on greenhouse-grown plants and therefore should be considered preliminary data until confirmed with field-grown plants. Regardless, this overall gross phenotypic characterization highlights several aspects of development that should be explored further for specific miRNA regulation.

fzt mutant plants are easily recognized due to their shorter stature, as well as their shorter and narrower leaves (B. Thompson, unpublished). In plants, cell size and/or cell number determines final organ size [26, 29]. We investigated whether *fzt* leaves had smaller cells or fewer cells to account for their smaller organ size. We first examined juvenile leaves, but did not see a significant difference in either the cell size between *fzt* mutant and normal sibling plants, and we therefore inferred there was a difference in cell number. We then further investigated by examining adult plants, where the organ size difference appears more prominent, but again we saw little difference between *fzt* mutant and normal sibling plants in cell size or cell number.

Cell number was determined by the number of cells in a given field of view, and because the size and number of the cells are comparable, then other considerations must be taken into account. This led to the interesting idea that cell proliferation might be perturbed in *fzt* mutant plants and therefore result in the smaller organ size [27].

Leaf growth is controlled by a combination of cell division and cell expansion. Cell division occurs in the pre-differentiation zone, which is found at the base of the emerging leaf and is composed of undifferentiated cells. Cell expansion occurs in the post-differentiation zone. The pre- and post-differentiation zones can be easily distinguished because the pre-differentiation zone lacks differentiated cell types, such as stomata complexes and epidermal hairs that are present in the post-differentiation zone [13; A.J. Wright, personal communication]. The reduced leaf size in *fzt* plants could be due to a smaller pre-differentiation zone or reduced rates of cell division in the pre-differentiation zone, resulting in fewer total leaf cells. To investigate the differences between the pre- and post-differentiation zones in normal and *fzt* mutant plants, I am using a combination of propidium iodide staining, which stains DNA, and tubulin antibodies to visualize mitotic spindles and the orientation of microtubules. These experiments will allow me to determine if there is a cell division defect in *fzt* leaves.

Furthermore, the orientation of microtubules specifies the direction of cell elongation [31], and therefore tubulin staining will indicate if cell expansion is aberrant in *fzt* plants.

CONCLUSIONS

In conclusion, we have shown that miRNAs are essential for proper vegetative development in maize plants. This pioneering study can lead to many possibilities of continuing to investigate the roles of miRNAs in maize vegetative development. One such experiment could be to determine the abundance of DICER-LIKE1 protein through Western blots. This experiment could be done to compare normal siblings and *fzt*, as well as comparing *fzt* mutants in different inbred backgrounds. We have seen a varying degree of phenotypic severity in different inbred backgrounds and visualizing this difference in regards to the mutated protein could help answer the cause of this phenomenon.

REFERENCES

1. Axtell, M. J., Westholm, J. O., & Lai, E. C. (2011). Vive la difference: Biogenesis and evolution of microRNAs in plants and animals. *Genome Biology*, *12*(4), 221. doi:10.1186/gb-2011-12-4-221
2. Becraft, P. W. (1999). Development of the leaf epidermis. *Current topics in developmental biology* (45th ed., pp. 1). San Diego: Academic Press.
3. Candela, H., Johnston, R., Gerhold, A., Foster, T., & Hake, S. (2008). The milkweed pod1 gene encodes a KANADI protein that is required for abaxial/adaxial patterning in maize leaves. *The Plant Cell*, *20*(8), 2073-2087. doi:10.1105/tpc.108.059709
4. Chen, X. (2009). Small RNAs and their roles in plant development. *Annual Review of Cell and Developmental Biology*, *25*, 21-44. doi:10.1146/annurev.cellbio.042308.113417
5. Chitwood, D. H., Guo, M., Nogueira, F. T., & Timmermans, M. C. (2007). Establishing leaf polarity: The role of small RNAs and positional signals in the shoot apex. *Development (Cambridge, England)*, *134*(5), 813-823. doi:10.1242/dev.000497
6. Chuck, G., Cigan, A. M., Saeteurn, K., & Hake, S. (2007). The heterochronic maize mutant Corngrass1 results from overexpression of a tandem microRNA. *Nature Genetics*, *39*(4), 544-549. doi:10.1038/ng2001
7. Chuck, G., Meeley, R., Irish, E., Sakai, H., & Hake, S. (2007). The maize tasselseed4 microRNA controls sex determination and meristem cell fate by targeting Tasselseed6/indeterminate spikelet1. *Nature Genetics*, *39*(12), 1517-1521. doi:10.1038/ng.2007.20
8. Chuck, G., Whipple, C., Jackson, D., & Hake, S. (2010). The maize SBP-box transcription factor encoded by tasselsheath4 regulates bract development and the establishment of meristem boundaries. *Development (Cambridge, England)*, *137*(8), 1243-1250. doi:10.1242/dev.048348

9. Dudley, M., & Poethig, R. S. (1993). The heterochronic Teopod1 and Teopod2 mutations of maize are expressed non-cell-autonomously. *Genetics*, *133*(2), 389-399.
10. Emery, J. F., Floyd, S. K., Alvarez, J., Eshed, Y., Hawker, N. P., Izhaki, A., et al. (2003). Radial patterning of arabidopsis shoots by class III HD-ZIP and KANADI genes. *Current Biology : CB*, *13*(20), 1768-1774.
11. Freeling, M., & Hake, S. (1985). Developmental genetics of mutants that specify knotted leaves in maize. *Genetics*, *111*(3), 617-634.
12. Howell, S. H. (1998). *Molecular genetics of plant development*. Cambridge: Cambridge University Press.
13. Hunter, C. T., Kirienko, D. H., Sylvester, A. W., Peter, G. F., McCarty, D. R., & Koch, K. E. (2012). Cellulose synthase-like D1 is integral to normal cell division, expansion, and leaf development in maize. *Plant Physiology*, *158*(2), 708-724. doi:10.1104/pp.111.188466
14. Juarez, M. T., Kui, J. S., Thomas, J., Heller, B. A., & Timmermans, M. C. (2004). microRNA-mediated repression of rolled leaf1 specifies maize leaf polarity. *Nature*, *428*(6978), 84-88. doi:10.1038/nature02363
15. Juarez, M. T., Twigg, R. W., & Timmermans, M. C. (2004). Specification of adaxial cell fate during maize leaf development. *Development (Cambridge, England)*, *131*(18), 4533-4544. doi:10.1242/dev.01328
16. Kidner, C. A., & Martienssen, R. A. (2005). The developmental role of microRNA in plants. *Current Opinion in Plant Biology*, *8*(1), 38-44. doi:DOI: 10.1016/j.pbi.2004.11.008
17. Lauter, N., Kampani, A., Carlson, S., Goebel, M., & Moose, S. P. (2005). microRNA172 down-regulates glossy15 to promote vegetative phase change in maize. *Proceedings of the National Academy of Sciences of the United States of America*, *102*(26), 9412-9417. doi:10.1073/pnas.0503927102
18. Liu, D., Song, Y., Chen, Z., & Yu, D. (2009). Ectopic expression of miR396 suppresses GRF target gene expression and alters leaf growth in arabidopsis. *Physiologia Plantarum*, *136*(2), 223-236. doi:10.1111/j.1399-3054.2009.01229.x

19. Manoli, A., Sturaro, A., Trevisan, S., Quaggiotti, S., & Nonis, A. (2012). Evaluation of candidate reference genes for qPCR in maize. *Journal of Plant Physiology*, *169*(8), 807-815. doi:10.1016/j.jplph.2012.01.019
20. Moose, S. P., Lauter, N., & Carlson, S. R. (2004). The maize macrohairless1 locus specifically promotes leaf blade macrohair initiation and responds to factors regulating leaf identity. *Genetics*, *166*(3), 1451-1461.
21. Moose, S. P., & Sisco, P. H. (1994). Glossy15 controls the epidermal juvenile-to-adult phase transition in maize. *The Plant Cell*, *6*(10), 1343-1355. doi:10.1105/tpc.6.10.1343
22. Nelson, J. M., Lane, B., & Freeling, M. (2002). Expression of a mutant maize gene in the ventral leaf epidermis is sufficient to signal a switch of the leaf's dorsoventral axis. *Development (Cambridge, England)*, *129*(19), 4581-4589.
23. Nogueira, F. T., Chitwood, D. H., Madi, S., Ohtsu, K., Schnable, P. S., Scanlon, M. J., et al. (2009). Regulation of small RNA accumulation in the maize shoot apex. *PLoS Genetics*, *5*(1), e1000320. doi:10.1371/journal.pgen.1000320
24. Nogueira, F. T., Madi, S., Chitwood, D. H., Juarez, M. T., & Timmermans, M. C. (2007). Two small regulatory RNAs establish opposing fates of a developmental axis. *Genes & Development*, *21*(7), 750-755. doi:10.1101/gad.1528607
25. Poethig, R. S. (2009). Small RNAs and developmental timing in plants. *Current Opinion in Genetics & Development*, *19*(4), 374-378. doi:10.1016/j.gde.2009.06.001
26. Reynolds, J. O., Eisses, J. F., & Sylvester, A. W. (1998). Balancing division and expansion during maize leaf morphogenesis: Analysis of the mutant, warty-1. *Development (Cambridge, England)*, *125*(2), 259-268.
27. Rodriguez, R. E., Mecchia, M. A., Debernardi, J. M., Schommer, C., Weigel, D., & Palatnik, J. F. (2010). Control of cell proliferation in arabidopsis thaliana by microRNA miR396. *Development (Cambridge, England)*, *137*(1), 103-112. doi:10.1242/dev.043067
28. Sakaguchi, J., & Fukuda, H. (2008). Cell differentiation in the longitudinal veins and formation of commissural veins in rice (*oryza sativa*) and maize (*zea mays*). *Journal of Plant Research*, *121*(6), 593-602. doi:10.1007/s10265-008-0189-1

29. Smith, L. G., Hake, S., & Sylvester, A. W. (1996). The tangled-1 mutation alters cell division orientations throughout maize leaf development without altering leaf shape. *Development (Cambridge, England)*, 122(2), 481-489.
30. Voinnet, O. (2009). Origin, biogenesis, and activity of plant microRNAs. *Cell*, 136(4), 669-687. doi:10.1016/j.cell.2009.01.046
31. Wright, A. J., Gallagher, K., & Smith, L. G. (2009). Discordia1 and alternative Discordia1 function redundantly at the cortical division site to promote preprophase band formation and orient division planes in maize. *The Plant Cell*, 21(1), 234-247. doi:10.1105/tpc.108.062810
32. Zhang, B., Pan, X., Cobb, G. P., & Anderson, T. A. (2006). Plant microRNA: A small regulatory molecule with big impact. *Developmental Biology*, 289(1), 3-16. doi:10.1016/j.ydbio.2005.10.036